Title
Kinetics and Dynamics Studies of Clathrate Hydrates

Author
Guo, Jin

Publication Date
2016

Peer reviewed|Thesis/dissertation

UNIVERSITY OF CALIFORNIA,
IRVINE

Kinetics and Dynamics Studies of Clathrate Hydrates
DISSERTATION

submitted in partial satisfaction of the requirements
for the degree of

DOCTOR OF PHILOSOPHY

in Chemistry

by

Jin Guo

Dissertation Committee:
Professor Rachel W. Martin, Chair
Professor Kenneth C. Janda
Professor Douglas J. Tobias

2016

DEDICATION

To

my parents,

Fuhai Guo and Shaohua Wang

For their endless love and support throughout my life.

TABLE OF CONTENTS

LIST OF FIGURES

LIST OF TABLES

ACKNOWLEDGMENTS

First and foremost, I would like to thank my advisor, Prof. Rachel W. Martin. It has been a great honor to be a "Probemonkey". I would never imagine to be here, Irvine, where I am currently positioned, writing this thesis if I did not have the short "beer talk" with Rachel during one of the Friday happy hour at Berkeley in 2010. There have been lots of inevitable ups and downs in research, but Rachel is always there to stay positive and her patience, support, and confidence I will always cherish. I would also like to thank my co-advisor Prof. Kenneth C. Janda. I am extremely grateful for the opportunity to participate in the research project in his lab. Ken is the most charismatic man I have ever met. His passion for science and the indefatigable good humor have always kept our scientific endeavors marching forward.

A significant portion of my graduate school days were spent with Dr. Suvrajit Sengupta. He is one of the most brilliant and supportive persons I have had the pleasure to learn from. Whenever and wherever there is a problem, he is always there to inspire me and generate endless great ideas. Since the first day he joined, Suv has effectively served as not only being a mentor to teach me theory and instrumentation, but also for being a tremendous friend to lend an ear in some of my dark moments when nothing seemed to be working.

My time in Martin lab has been a gift to me and it has been a pleasure to work with so many bright and kind minds in such an enjoyable atmosphere. I would like to thank Kelsey for being a such good "cryogen-fill" buddy that we both never had to flee to another continent in the past five years. And I also thank John, Jan, and Kyle for being the new "cryogen-fill triangle" and I wish all the best to them. Additionally, I would like to thank Domarin, who navigated the challenges of the first year with me and also played den mother to all of us for managing and

organizing all the lab activities. There have been many others in the group who supported me in many ways and I would like to express my gratitude to all the members of the Martin lab, including Carolyn, Natasha, David, Megha, and Vy for the valuable discussion and constructive suggestions when I was preparing my advancement and defense talks.

While I spent most of time in the Martin lab, I am also thankful for my peers in Janda Lab. The kinetic work presented here could not have been accomplished without the help of Jaruwan Amtawong, who made huge impacts on helping and guiding me set up the instruments and start the project. I would also like to thank Prof. Everly Fleischer for being a constantly valuable source of many inspirations and ideas for the entire hydrate lab. From him, I knew I would never have the excuse to stop learning new things for the rest of my life.

I would also like to thank my thesis committee member: Prof. Douglas J. Tobias, and advancement committee members: Prof. Vladimir A. Mandelshtam, Prof. Sergey Nizkorodov, Prof. Athan J. Shaka, Prof. Andrej Luptak, and Prof. Michael Dennin for their critical feedbacks.

No doubt, there are uncountable failures in graduate school. I got ninety-nine problems but friendship ain't one. The most valuable asset that I have harvested in graduate school is friendship and I will always be indebted to my friends at UCI. Mya Le-Thai, Julie Hsu, Eric Wong, Paolo Reyes, Jose (Raul) Ocampo, and I quickly became close friends in the beginning of the 2011 Fall and the gang got expanded after Suv joined. I still fondly remember our first year, struggling through mid-night in NS I for Prof. Burke's DFT homework, staying all day long in Mya's apartment before the finals, and cheering some small accomplishments (or just wanting to drink) in those beer/soju/K-BBQ nights. Through these years, the vast majority of my learning, not just for research but also for life experiences, has been from interacting with these bright, passionate, and selfless scientists that I will cherish forever.

It is amazing to see how one's life is changed from some arbitrary choices and random incidents. I would never imagine to attempt this journey without the encouragement from two people at Berkeley. If there was not a sign with capitalized "Free Lunch on Friday !" in the Stanley hall, I would probably never have my first brush with the beauty of NMR in Pines lab. As a new international student with a not-so-great GPA and zero research experience, Prof. Alex Pines took a chance and gave me the opportunity to experience the academic research in his lab. I greatly appreciated all his support to ensure the research performed is always exciting and cutting-edge for us undergraduates and I ended up working in his lab for two years. Another important mentor that I would like to thank is Dr. Xin Zhou. Since the first day I joined the Pines lab, he has been generous and supportive to me, both academically and personally, even till now. His dedications and enthusiasms in science gave me the sense that the world of research was quite interesting and doing NMR was a choice made thanks to his wonderful influence, to whom I own more than I can put into words.

Lastly and finally, I am deeply and sincerely grateful to my family. Ten years has been a long journey since the first day I started my US adventure in 2007. At this moment, I have nothing else to say but thanks to my parents. Without their endless love and support, I would never be what I am now. This journey will hold much more meaning if I have ever made them feel somewhat proud of me.

CURRICULUM VITAE

Jin Guo

EDUCATION

Doctor of Philosophy in Chemistry 2016
University of California, Irvine Irvine, CA

Bachelor of Science in Chemical Engineering 2011
University of California, Berkeley Berkeley, CA

WORK EXPERIENCE

Graduate Research Assistant 2011-2016
University of California, Irvine Irvine, CA

Graduate Teaching Assistant 2011-2016
University of California, Irvine Irvine, CA

Research Assistant 2009-2011
University of California, Berkeley Berkeley, CA

PUBLICATIONS

1. **Jin Guo**, Jaruwan Amtawong, Suvrajit Sengupta, Rachel W. Martin and Kenneth C. Janda "Kinetics of Fluoromethane Clathrate Hydrate Formation from CH_3F Gas and Methanol Doped Ice Particles." *In Preparation.*

2. Jaruwan Amtawong, Michael T. Nguyen, Nicole C. Carrejo, **Jin Guo**, Suvrajit Sengupta, Everly B. Fleischer, Rachel W. Martin, and Kenneth C. Janda. "Kinetics of Trifluoromethane Clathrate Hydrate Formation from CHF_3 Gas and Ice Particles" *Under Revision. The Journal of Physical Chemistry C*.

3. Jaruwan Amtawong, **Jin Guo**, Jared S. Hale, Suvrajit Sengupta, Everly B. Fleischer, Rachel W. Martin, and Kenneth C. Janda. "Propane Clathrate Hydrate Formation Accelerated by Methanol." *The Journal of Physical Chemistry Letters* (2016).

4. Suvrajit Sengupta, **Jin Guo**, Kenneth C. Janda, and Rachel W. Martin."Exploring Dynamics and Cage-guest Interactions in Clathrate Hydrates using Solid-state NMR." *The Journal of Physical Chemistry B* (2015).

AWARDS

Lawrence Berkeley National Laboratory Summer 2010 Research Award 2010
College of Chemistry Stanley and Alice Thompson Undergraduate Research Award 2010

ABSTRACT OF THE DISSERTATION

Kinetics and Dynamics Studies of Clathrate Hydrates

By

Jin Guo

Doctor of Philosophy in Chemistry

University of California, Irvine, 2016

Professor Rachel W. Martin, Chair

Clathrate hydrates are a class of compounds in which small guest molecules, such as methane, ethane, tetrahydrofuran, *etc.* are encapsulated within a hydrogen-bonded host water cages. In the oil industry, vast deposits of methane hydrates in deep ocean and permafrost have received great interest as a potential energy source. However, methane hydrate formation can potentially block the transmission pipelines in deep see drilling which may lead to catastrophic economic losses from the flow assurance failures. Therefore, understanding the fundamental mechanisms of gas hydrates formation, decomposition and inhibition is the key for their safe and economical use as a potential energy source and natural gas storage. The effect of low concentrations of methanol on the clathrate hydrate formation kinetics were studied in this thesis. The catalytic effects from methanol were observed on propane hydrate formation but inhibitory effects were found in fluoromethane hydrate formation. We postulate that the catalytic activity of methanol is dependent on the nature of the guest gas itself. Moreover, one of the fascinating properties of the clathrate hydrate structure is that the water molecules of host lattice completely satisfy the

hydrogen-bonding requirement, so the interactions between the guests and host cages are mainly due to van der Waals forces rather than hydrogen bondings. Within the cages, the trapped guest molecules have limited translational mobility but may retain rotational and vibrational freedom. From the standpoint of physical chemistry, the dynamics of the guest and host molecules is an excellent material to study and the motion of the guest molecules within the cages is not well understood. In this thesis, the dynamics of tetrahydrofuran (THF) and cyclopentane (CP) guests in the hydrate cages above 200 K were investigated by magic angle spinning (MAS) solid-state NMR. The barrier to guest motion of CP is much lower than THF indicating the existence of hydrogen bonding interactions between THF guest and cage water molecules above 200 K.

CHAPTER 1: Clathrate Hydrates

1.1 Introduction to Clathrate Hydrates

According to IUPAC, "clathrates" are defined as "inclusion compounds in which the guest molecule is in a cage formed by the host molecule or by a lattice of host molecules".[1] When the host lattice is made up of water molecules, they are referred to as clathrate hydrates, and in the special case when the guest molecule is a gas under normal atmospheric conditions, they are commonly called gas hydrates. Gas hydrate was first discovered by Sir Humphry Davy in 1810, when he discovered that a mixture of chlorine and water solidified well above the ice melting point.[2] Since his discovery, various clathrate hydrates have been studied. Early studies on clathrate hydrates focused on identifying the guest molecules that form hydrate and the conditions under which they occur. The first phase diagram of gas hydrate was presented by Roozeboom in 1884.[3] Clathrate hydrates (CHs) can be formed when hydrophobic guest molecules and host (water) molecules come into contact at low temperature and high pressure. Due to their strong hydrogen bonding interactions with water lattice, the hydrophilic molecules often hardly form simple and stable CHs on their own.[4] However, a hydrophilic molecule may be captured in a double hydrate system if it is put into the water lattice with the help of hydrophobic guest molecules.[5,6] Since both water-miscible and water-immiscible guests can form hydrates, the stability of CH structure is determined by the balance between hydrophilic and hydrophobic guest-host interactions.[7]

In clathrates, the whole water molecule network is linked by hydrogen bonding to form the "building blocks" of cavities to encage guest molecules (**Figure 1**). The common CHs are categorized into three major types of crystal structure, cubic structure (CS) I, cubic structure (CS) II, and hexagonal (H) structure. The clathrate hydrate structure is often recognized by the

connection of the cavities. In the CS-I structure, the 5^{12} building blocks are linked together through their vertices.[8,9] It has two small dodecahedral (5^{12}) cages and six large tetrakaidecahedral ($5^{12}6^2$) cages with a total of 46 water molecules in a unit cell. The small guest molecules with diameter between 0.4 and 0.55 nm can fit in small (5^{12}) cages, such as methane and hydrogen sulfide.[10] The CS-II structure is formed when the building blocks are joined to others through face sharing, and it has sixteen dodecahedral (5^{12}) cages and eight large hexakaidecahedral ($5^{12}6^4$) cages with a total of 136 water molecules in a unit cell.[11] This structure generally contains larger guest molecules with diameters ranging from 0.6-0.7 nm, such as propane and tetrahydrofuran that only fit into the large $5^{12}6^4$ cages.[12,13] Guest molecules with diameter less than 0.4 nm such as oxygen, nitrogen, and the noble gases, tend to favor the structure H hydrates due to the large fraction of small 5^{12} cages.[14,15] However the larger guest molecules with diameters between 0.8 and 0.9 nm, such as adamantane and 2, 2-dimethylpentane, can still fit into structure H when they are accompanied by small guest molecules to form double hydrate system.[16,17]

a

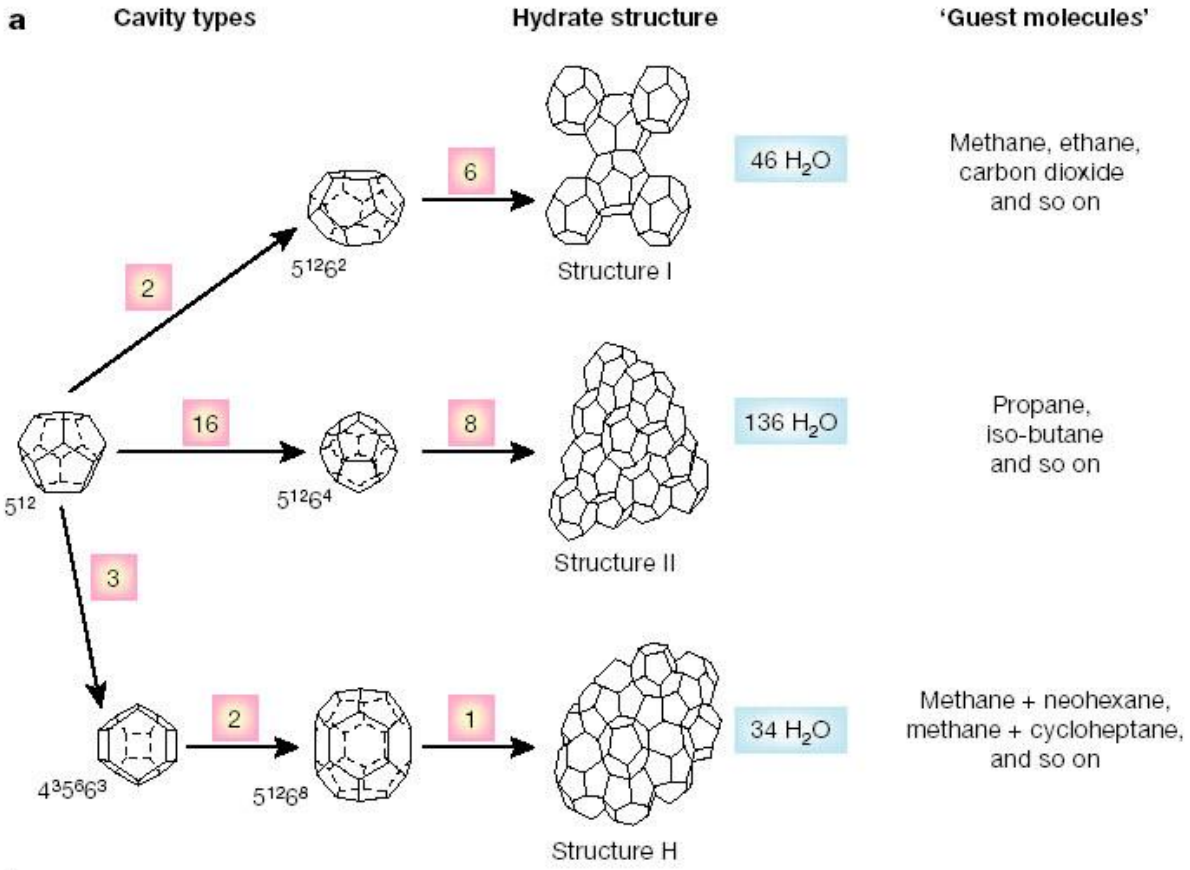

b

Hydrate crystal structure	I		II		H		
Cavity	Small	Large	Small	Large	Small	Medium	Large
Description	5^{12}	$5^{12}6^2$	5^{12}	$5^{12}6^4$	5^{12}	$4^35^66^3$	$5^{12}6^8$
Number of cavities per unit cell	2	6	16	8	3	2	1
Average cavity radius (Å)	3.95	4.33	3.91	4.73	3.91†	4.06†	5.71†
Coordination number*	20	24	20	28	20	20	36
Number of waters per unit cell	46		136		34		

*Number of oxygens at the periphery of each cavity.
†Estimates of structure H cavities from geometric models.

Figure 1. The properties of three common clathrate hydrate structures.[8] Reproduced with permission from reference 8.

1.2 Historical Perspective of Gas Hydrates in the Oil Industry

The ability to trap natural gases makes CH a good potential energy source. Colossal deposit of natural gas clathrate hydrates are fond in the deep ocean and permafrost. Following the discovery of the first natural gas hydrate deposit in Russia in 1960s, kinetic study of gas hydrate formation has attracted great attention. Understanding the kinetic and thermodynamic properties of CHs is the key for their economical use as a potential energy source, gas storage systems, and the transportation of fuels through pipelines. Methane is one of the most common clean energy sources, and most of its hydrate form occurs naturally in permafrost regions and deep ocean continental margins.[18] The inventory of methane hydrate is estimated to be twice the amount of all other fossil fuels combined.[8] For example, **Figure 2 (a)** shows the currently known inventory of methane hydrate in permafrost regions and through deep sea deposits near the coasts all over the world. Although the equilibrium thermodynamic and structural properties of gas hydrates have been well characterized over the years, the fundamental understanding of the mechanisms of gas hydrate formation, decomposition and inhibition is still quite unclear. It becomes even more critical for the development and improvement of technologies for the potential extraction of substantial quantities of methane from these deposits offers an attractive solution to addressing the energy needs for the future.

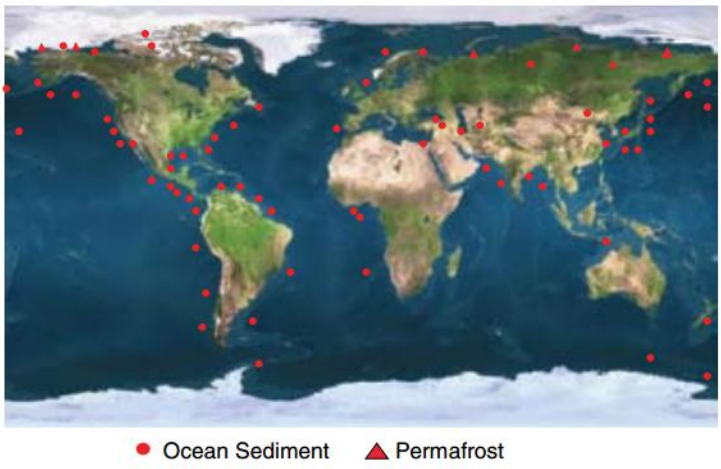

Figure 2 (a). Global distribution of confirmed or inferred gas hydrate sites, 1997 (courtesy of James Booth, U.S. Geological Survey). Gas hydrate is probably present in essentially all continental margins.[18] Reproduced with permission from Reference 18.

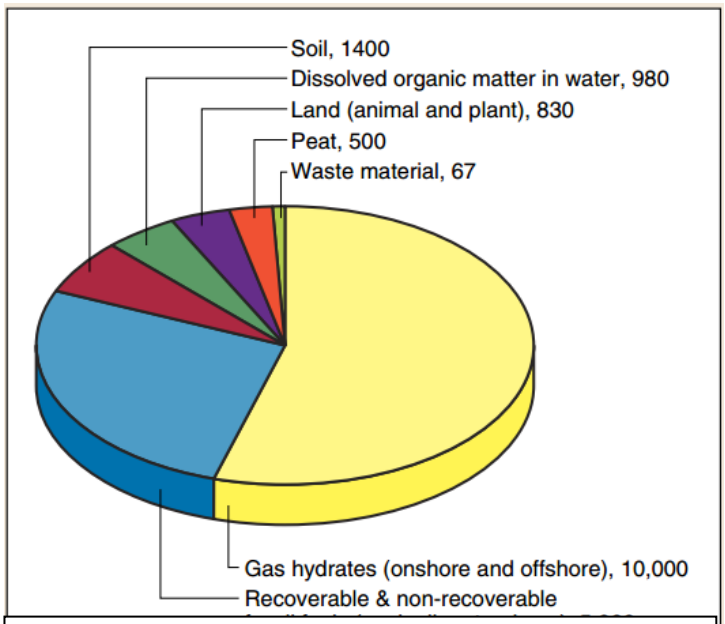

Figure 2 (b). Distribution of organic carbon in Earth's crust in gigatons.[18] Reproduced with permission from Reference 18.

However, the spontaneous formation of gas hydrates can potentially block pipelines which may lead to costly flow assurance failures in the oil industry.[9] The earliest study dealing with the risk can be traced back to mid-1930s, when it was found that natural gas hydrates were blocking gas transmission lines frequently at temperatures above the ice point.[19] This discovery essentially initiated intense research programs by the oil and gas industry over the next century for the purpose of preventing and regulating the formation of gas hydrates in transmission pipelines. In oil industry, gas hydrates are known to be the primary flow assurance issue in deepwater drilling.[20] Undesired water in oil and gas wells combines with hydrocarbons that are in the hydrate guest size range, to form hydrates especially under low temperature and high-pressure conditions. Eventually hydrates plug the transmission lines which leads to costly and possibly dangerous production stoppage. Sometimes it takes months to remove the hydrate plug. Gas pipeline blockage from gas hydrates is still an important industrial problem that leads to safety hazards for personnel and production equipment, and substantial economic risks. In order to prevent the costly blockages, finding a way to maintain the delivery system outside the hydrate stability range is an urgent need. Therefore, understanding of the hydrate formation mechanisms is the indispensable step to help the industries find the solution to prevent hydrate formation.

1.3 Hydrate Formation Inhibitors

In the current petroleum and gas industries, the technology employed to prevent of gas hydrate formation in pipelines consists of the introduction of inhibitors. Two major types of inhibitors are widely applied for CH suppression, a large concentration of thermodynamic hydrate inhibitors (THIs), such as alcohols and glycols, and a low dosage of kinetic hydrate inhibitors (KHIs), such as PVP and PVCap.[10] The kinetic hydrate inhibitors (KHIs) are used at low concentration from 0.1 to 1.0 wt%. The KHIs act primarily as gas hydrate anti-nucleators

and they delay the hydrate formation to longer times than the residence time of the gas within the hydrate-prone section of pipeline.[21] These low dosage inhibitors can offer significant economic and environmental advantages compared to the traditional thermodynamic inhibitors. However, some studies have shown that KHIs may accelerate the hydrate growth, commonly referred to "catastrophic growth".[22,23] This phenomenon is facilitated by the capillary movement of water molecules across the formed hydrate layer to the water/gas interface which essentially enhances further growth after the initiation.[24] For thermodynamic hydrate inhibitors (THIs), the inhibition effect is due to the shift of the phase boundary of hydrate formation to lower temperature and/or higher pressures by adding a sufficient amount of chemicals.[25] Among all inhibitors, methanol has been extensively used because it is assumed that methanol does not participate in the formation of CHs.[19] However, the methanol inhibits CH formation only when the concentration is large, up to 40% by volume.[26] Therefore, when the drilling and production occur in the deep ocean under severe temperature and pressure conditions, the amount of inhibitor required is huge. For example, in a small gas reservoir, there is approximately 3.155×10^4 kilogram of water content in the gas flow per day. For each kg of water, it requires 0.65kg of methanol to prevent the hydrate formation, which means the usage of 2.4×10^4 L methanol per day. With the methanol cost of $0.56/L, a yearly cost to prevent hydrate formation is around $5 million for a small field, which is definitely not a trivial amount[25]

1.4 Catalytic Effects from Methanol

Although methanol has been widely employed as an inhibitor, recent studies have shown some interesting results in which methanol can participate in the formation of CHs. For example, the strong guest-host interactions from hydrogen bonding interfere with the hydrophobic necessity of CH formation.[7] Also, unlike larger alcohols, the hydrophobic region of methanol is

relatively too small to stabilize the formation of CHs. Therefore, methanol should not form CHs on its own.[27–30] However, some researchers have shown that methanol can form CHs with water,[31,32] or form double hydrates with other small hydrophobic molecules,[4,33–37] or form hydrates with a modified lattice framework.[38] An FT-IR study showed that a simple methanol clathrate is not thermodynamically stable but it can be included in the small cages of the CS-I and CS-II double hydrates of ethylene oxide and THF, respectively.[4] Blake *et al.* experimentally observed the formation of CS-II methanol CHs from annealing of amorphous mixtures of water and methanol at high concentrations.[31] During the formation, the presence of crystalline CHs and the segregation of methanol to form amorphous boundaries were captured by electron diffraction. Shin and Ripmeester used X-ray diffraction and NMR to show how a methanol molecule is incorporated into the small cages of CS-II THF CH. In the host lattice, an oxygen atom from water is replaced by methanol and leaves the methyl group sitting toward the center of the cage.[36] They also found that the amount of methanol incorporated into the host lattice depends on the preparation methods. A large quantity of methanol (49 %) was included during the rapid freezing formation process in which the THF/H_2O/CH_3OH solution was quenched by liquid nitrogen. And only 4.4% of methanol was incorporated in the slow grown single crystal. In the ammonium fluoride modified lattice, methanol was reported to be a sole guest with 100% cage occupancies for CS-I large cages and 73% for CS-I small cages.[38] Since the ammonium and fluoride ions replace two adjacent waters in the host lattice, the strong interactions between methanol and the ammonium and/or fluoride ions were speculated to account for the stability of the methanol CH.[38]

The role of methanol as a catalyst in CH formation has been intensely discussed as well.[33–35,39] Recently, Ripmeester's group has presented the catalytic effect of low methanol

concentrations on the formation of CS-I methane CHs from frozen water-methanol mixtures.[34] Based on the assumption that methanol solution coated on the ice surface during formation, their molecular simulations showed that Bjerrum defects were created in the host lattice frame due to the strong interactions between methanol and water molecules on the ice surface, which eventually facilitated the catalytic effect. This result is also supported by another *in situ* study from Devlin.[35] They adopted an all-vapor aerosol approach in low temperature and pressure range. Under these conditions, 100% conversion of methanol-carbon dioxide and methanol-acetylene double hydrates was achieved by the addition of methanol vapor in less than one second. Since the time scale of CH formation was extremely quick in this study, the increased formation rate was assumed to be mostly controlled by the induction and stabilization of defects that enhance molecular transport through empty cages. These contradicting studies suggest that the behavior of methanol in CH formation is quite interesting and not well understood. It has left many open questions and attracted researchers to explore the microscopic mechanisms through which methanol influences CH formation or inhibition.

In the following chapters, kinetics of propane hydrate and fluoromethane hydrate formation with methanol doped ice will be investigated and discussed in greater details. In addition, dynamics of guest-cage interactions in clathrate hydrates will be presented in Chapter 4.

CHAPTER 2: Kinetics of Propane Hydrate Formation with Methanol Doped Ice

The motivation for this project is to investigate the catalytic effect of ultra low concentration methanol on CH formation from frozen methanol-water mixtures. Propane gas was chosen as the guest because of its propensity to form CH under moderate conditions and because its formation kinetics have been substantially investigated by the current techniques in various hydrate forms.[40–42] Rivera *et al.* found that in the early stages of propane CH formation, the formation rates have a negative correlation with temperature, yielding a negative activation energy.[41] As with propane hydrate formation, difluoromethane hydrate formation also has a strong negative temperature dependence characteristics of a negative activation energy and the formation rate and the yield is dependent on the gas flow rate.[42] Propane has also been employed as a co-guest to study the role of methanol as a guest in CS-II CH.[36] An NMR study showed the methyl portion of methanol resided in the small cage while the hydroxyl portion was incorporated in the water lattice, distorting the adjacent large cages containing propane. Besides its interesting molecular dynamic properties, propane is one of the major constituents of the natural gas clathrates and common structures found in oil and gas pipelines. Thus, the kinetic study of ice-to-hydrate formation of propane is significant in terms of understanding the reaction mechanism when methanol participates in the formation as a catalyst or inhibitor. For practical purposes, this might be useful to prevent the formation of clathrate blockages in low temperature environment in oil industry.

2.1 Shrinking Core Model

With these interesting studies from the literature, the role of methanol in CHs formation has attracted many researchers and also opened up many fascinating questions. The limited

knowledge of hydrate formation and decomposition can create many issues including irreproducibility and slow production methods.[43] The main challenges in the field are the formation kinetics and the complexity of the dynamics between gas molecules and liquid water during the formation process. Several kinetic models have been developed to describe a simpler case of CH formation in which ice particles are exposed to gas molecules at appropriate pressure and temperature.[4,44] The "shrinking core model" has been extensively studied and used to describe the formation kinetics of clathrate hydrates. This model was first proposed as two stages by Jander in 1927 for the formation of methane and carbon dioxide CHs.[45] Then it was further developed and expanded by adding a third stage that accounted for the existence of pores on the gas hydrate shell by Staykova *et al.* in 2003.[46] The model consists of three stages: The first stage (Stage I) is the initiation of gas hydrate shell formation surrounding the surface of the ice particle. The second stage (Stage II) is the mass transfer process, in which ice and/or gas enter through the hydrate shell pores to grow more CHs. The third stage (Stage III) describes how ice and/or water diffuse through the hydrate layer when the ice surface is entirely covered. It is important to note that the definition of the three reaction stages is purely empirical, rather than microscopic.

2.2 Results and Discussion

In this study, the growth kinetics of propane CH with methanol is described on the basis of the three-stage shrinking core model in which the water-methanol mixture particles are exposed to the propane gas. In this experiment, propane gas passes through a needle valve into the ice particles at 253K in the reaction cell. Initially the cell pressure rises as gas fills up the reaction vessel. Then a pressure drop in the reaction cell is observed even though the gas is continuously added to the cell. This is because at this stage the enclathration of the gas molecules is initiated,

and the gas is consumed by the ice faster than the needle valve introduces new gas into the system. **Figure 3 (a)** shows a pressure versus time profile and the top dark blue curve is a reference run for which the reaction cell contains 10mL of fine sand rather than ice. Since no CH is formed, the pressure of the reference run rises monotonically until it reaches the regulator pressure of 0.17 MPa as expected. The propane gas flow rate can be determined from the slope of the curve. The second red curve is the experimental run with pure ice. A monotonic increase in pressure stops at a threshold 0.15 MPa where the reaction takes place and a small pressure decrease is observed afterwards due to the full usage of maximum available nucleation sites in which the gas uptake rate of the ice particles is greater than the flow rate of the gas into the reaction cell. This fast CH formation period is referred to Stage I, in analogy to the shrinking core model. The other four curves in **Figure 3 (a)** are the data obtained from the experimental runs of various methanol concentrations ranging from 0.016 to 1 wt% in frozen water-methanol mixtures. At the lowest concentration 0.016% sample, which is less than one part per ten thousand mole ratio, the initiation pressure drops from 0.15 MPa to 0.13 MPa compared to the pure ice sample. For the highest methanol concentration at 1%, the initiation pressure drops to 0.089 MPa. The initiation pressures of other two intermediate methanol concentrations are slightly higher than the 1% sample. Numerical data for the initiation pressure and other kinetic data are reported in Table 1. From the results we obtained, the variation in the number of nucleation sites for the 1%, 0.25%, and 0.063% concentrations is not significant. However, for the lowest concentration sample 0.016%, the reaction occurs at a noticeably higher pressure approaching that of the pure ice sample. But it is clear that the reactions with methanol doping occur at much lower pressures than pure ice, contrary to the inhibition effect of methanol as a thermodynamic inhibitor for CH suppression.

Thereafter, the reaction rate reaches an equilibrium with the gas flow rate after the initial pressure drop of Stage I and the pressure remains constant for about an hour. In this reaction regime, most surface ice particles have been converted into CH, but there are some particles that still rapidly react with the gas. This reaction stage is referred to Stage II. For the 1% methanol sample, the Stage II pressure is 0.08 MPa, only slightly higher than the propane hydrate vapor pressure. At the lowest concentration (0.016%), the minimum of the Stage II pressure drops from 0.13 MPa to 0.11 MPa, compared to the pure ice sample. Similarly, the Stage II pressures of the two intermediate methanol concentrations are only slightly higher than that of the 1% sample.

From **Figure 3 (a)**, it is hard to distinguish the differences in duration of Stage II, especially for the 0.063%, 0.25%, and 1% samples. It indicates that the hydrate coverage on the surface is very similar for these concentrations so the Stage II duration is almost independent of methanol concentration. It is also important to note that the duration of Stage II in this study is considerably shorter compared to the previous kinetic study of propane CH.[41] For example, in this study Stage II of the reaction for the pure ice sample lasts for about 1.5 hours while the Stage II of the reaction for previous propane study is more than 8 hours at similar temperature and particle size. The gas flow in this study is set at much higher rate than the previous propane study and the effect of gas flow rate on the growth kinetics has been discussed in a paper describing the kinetics of difluoromethane CH by our group.[42] In the study, the experiment demonstrates that a faster initial reaction rate is caused by a fast flow rate, but the reaction stalls sooner than a slower flow rate experiment. The hypothesis is that the faster flow rates may form a more uniform clathrate shell which obstructs the further contact and reactions of gas molecules and fresh ice. The use of the high flow rate could be the reason for the significantly short duration of Stage II in this current experiment compared to the previous study by Rivera *et al.*.[41]

As more ice particles are covered by hydrate shell, the gas molecules and ice particles hardly have a chance to approach each other to facilitate the reactions. A slow diffusion of the propane and/or water molecules through the hydrate shell pores dominates this reaction regime, which is referred to as the Stage III regime. A cell pressure increase is observed from all four curves in **Figure 3 (a)** due to the decrease in the reaction rate. In our experiments, we seldom waited for the completion of Stage III because the diffusion process is extremely slow. Therefore, the labeling of Stages I, II, and III is in analogy with the shrinking core model as they were defined empirically rather than microscopically.

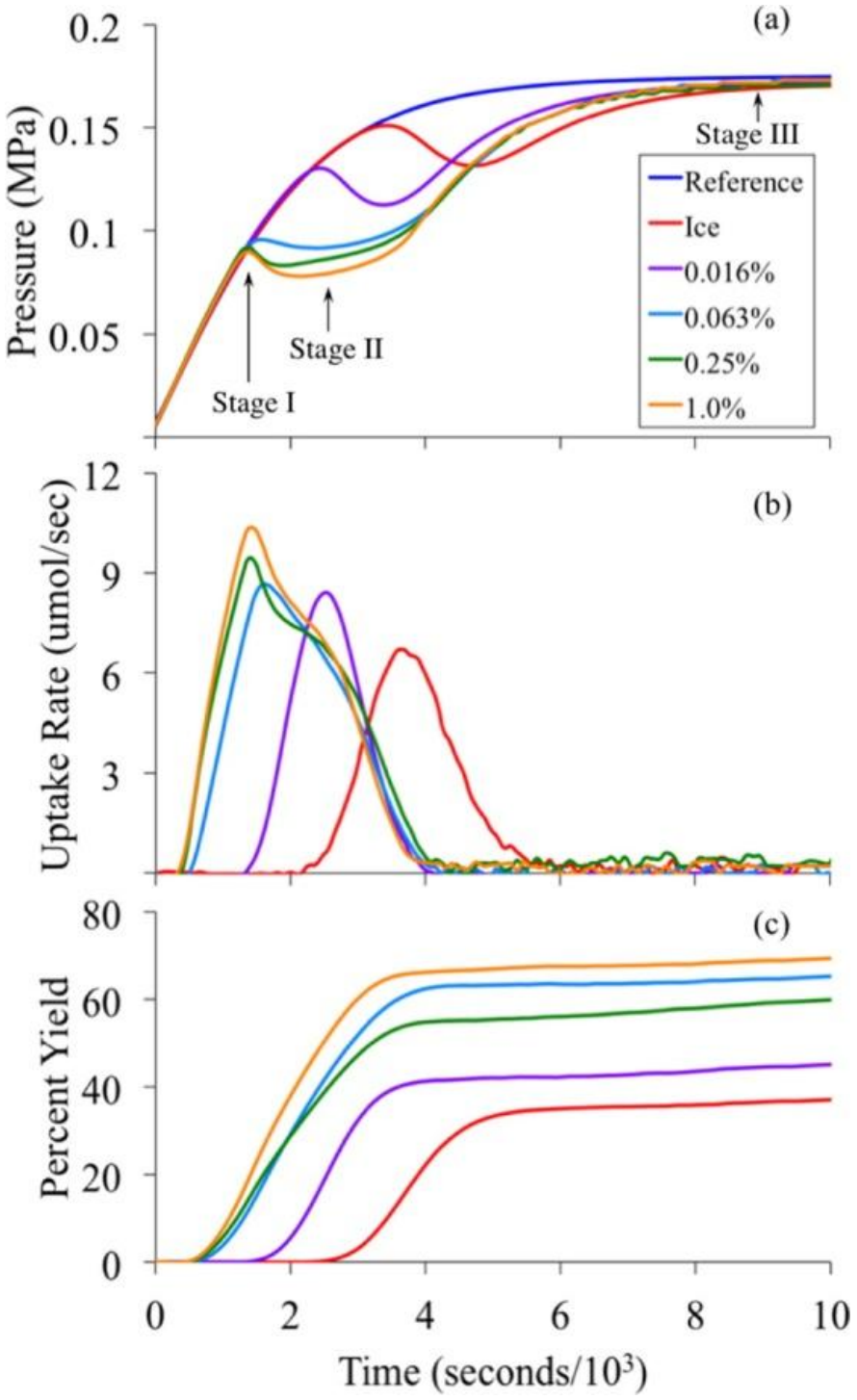

Figure 3:
(a) Pressure versus time profile of a reference run, a pure ice sample, and 4 experimental runs of methanol doped ice concentrations at 253K. **(b)** Uptake rate versus time. **(c)** Percent yield profile.[48]
Reprinted with permission from Reference 48. Copyright (2016) American Chemical Society

Because the uptake rate of gas into ice is dependent on the pressure difference across the needle valve, it can be determined by measuring the gas flow rate and the change of pressure in the reaction cell when clathrate forms. By using Peng-Robinson equation, the pressure is first converted into the number of moles:

$$PV = ZnRT \qquad (1)$$

where V is the volume of the reaction cell occupied by propane, Z is the compressibility factor as a function of pressure and temperature, P is the pressure of the gas inside the reaction cell which can be converted into the number of moles n. R is the ideal gas constant, and T is the average temperature. Then the uptake rate of the reaction can be derived by using the following formula:

$$\frac{dn_m}{dt} = \frac{dn_{cell}}{dt} - \frac{dn_{clathrate}}{dt} \qquad (2)$$

where $\frac{dn_m}{dt}$ is the rate of change of the moles of propane calculated from the measured pressure change for an experimental run, $\frac{dn_{cell}}{dt}$ is the flow rate of the propane gas into the cell calculated from a reference run, and $\frac{dn_{clathrate}}{dt}$ is the uptake rate of propane into clathrate.

Figure 3 (b) shows the results converted to uptake rate of propane versus time at various methanol concentrations. The maximum uptake rate of 1% sample is about 50% higher than that of the pure ice, even though the peak uptake rate of 1% occurs at a considerably lower cell pressure than that of the pure ice sample in **Figure 3 (a)**, 0.089 MPa versus 0.15 MPa respectively. For the lower concentration methanol samples including 0.063%, 0.016%, and pure ice, the negative slope regions of the uptake rate curves are slightly different from the higher concentration. The uptake rate of lower concentration samples rapidly decrease after they reach the maxima. However, for the 1% and 0.25% samples, there is a shoulder region that appears at

~$3x10^3$ s right after the sharp decrease in uptake rate that indicates a slower reaction rate followed.

If we attribute the positive slope region of the uptake rate curves to the encounter between gas and ice particles and the negative slope region to Stage II of formation, our data imply that the higher concentration samples would have higher fractions of propane populated near the ice surface than the lower methanol concentration and pure ice samples at the same reaction time. The driving force for the reaction initiation is very high which leads to a fast formation of the hydrate and a high maximum uptake rate during Stage I. Unlike the lower methanol concentration samples, the 1% and 0.25% samples both have shoulder regions in the uptake rate curves that clearly indicate that the reaction is slowed down. In this region, even though the hydrate shell has covered most of the ice surface, the gas absorption is still carried on by the contact between gas and ice particles which essentially facilitates a slight uptake rate decrease. In Stage III, all reactions dramatically slow down as this stage may be independent of the methanol concentration. This suggests that the enhancement of the initial propane absorption onto the ice surface is solely due to the catalytic effect of the methanol.

By integrating the uptake rate curve over time or $\frac{\mathrm{dn_{clathrate}}}{\mathrm{dt}}$, the total amount of propane consumed for CH formation can be determined. The yield of the propane CH can be obtained by assuming only the large $5^{12}6^4$ cages of CS-II structure are occupied, with a water to propane ratio (hydration number) of 17. In **Figure 3 (c)**, the higher methanol concentration samples tend to have higher percent yield. In the case of our experiment, we primarily focused on the Stage I and II reaction regimes, and the percent yield is 66% for the 1% methanol sample versus 35% for the pure ice sample at the end of Stage II. Again, the intermediate methanol concentration samples demonstrate intermediate results for maximum uptake and percent yield.

So far, the effects of methanol doping are quite surprising. Therefore, the reproducibility of this study required verification. **Figure 4** shows the three runs of concentration of 0.063% sample. Given the simplicity of our technique, especially with respect to particle production and size sorting, the reproducibility of the results is quite satisfying. The three data sets are similar, as the initial pressure rise in Stage I ranges from 0.095 to 0.098 MPa, the maximum uptake rates are from 8.2 to 8.7 μmol/s, and the percent yield ranges from 61% to 69%. It is clear to see that the duration of Stage II has a great effect on the final percent yield variation. From Table 1, the growth kinetics of the 0.063% and 0.025% samples are indistinguishable. Repeated experiments were also conducted on the 0.25% concentration samples. As expected, the results are reproducible.

Table 1. Numerical Data of the Growth Kinetics of Propane Clathrate Hydrate[a]

Methanol Concentration (wt %)	Mass of Ice (g)	Initiation Pressure (MPa)	Maximum Uptake Rate (μmol/s)	% Conversion[b]	Duration of State I and II ($s/10^3$)
0 (pure ice)	9.3	0.15	6.7	35	5.5
0.016	8.7	0.13	8.4	41	3.8
0.063	8.5(0.3)	0.096(0.002)	8.6(0.2)	63(4)	4.3(0.3)
0.25	11(1.6)	0.092(0.001)	9.5(0.3)	55(8)	4.0(1.0)
1.0	9.3	0.089	10	66	3.8
0.08 (g)[c]	8.5	0.093	8.1	55	4.0

[a] The numbers in the table are for the representative data. When more than one run was performed, the number in parentheses is the deviation between the reported value and the extreme values for the least significant figure.
[b] Percent yield reported here corresponding to the time listed in the final column.
[c] Methanol was added separately (see text for more information).[48]

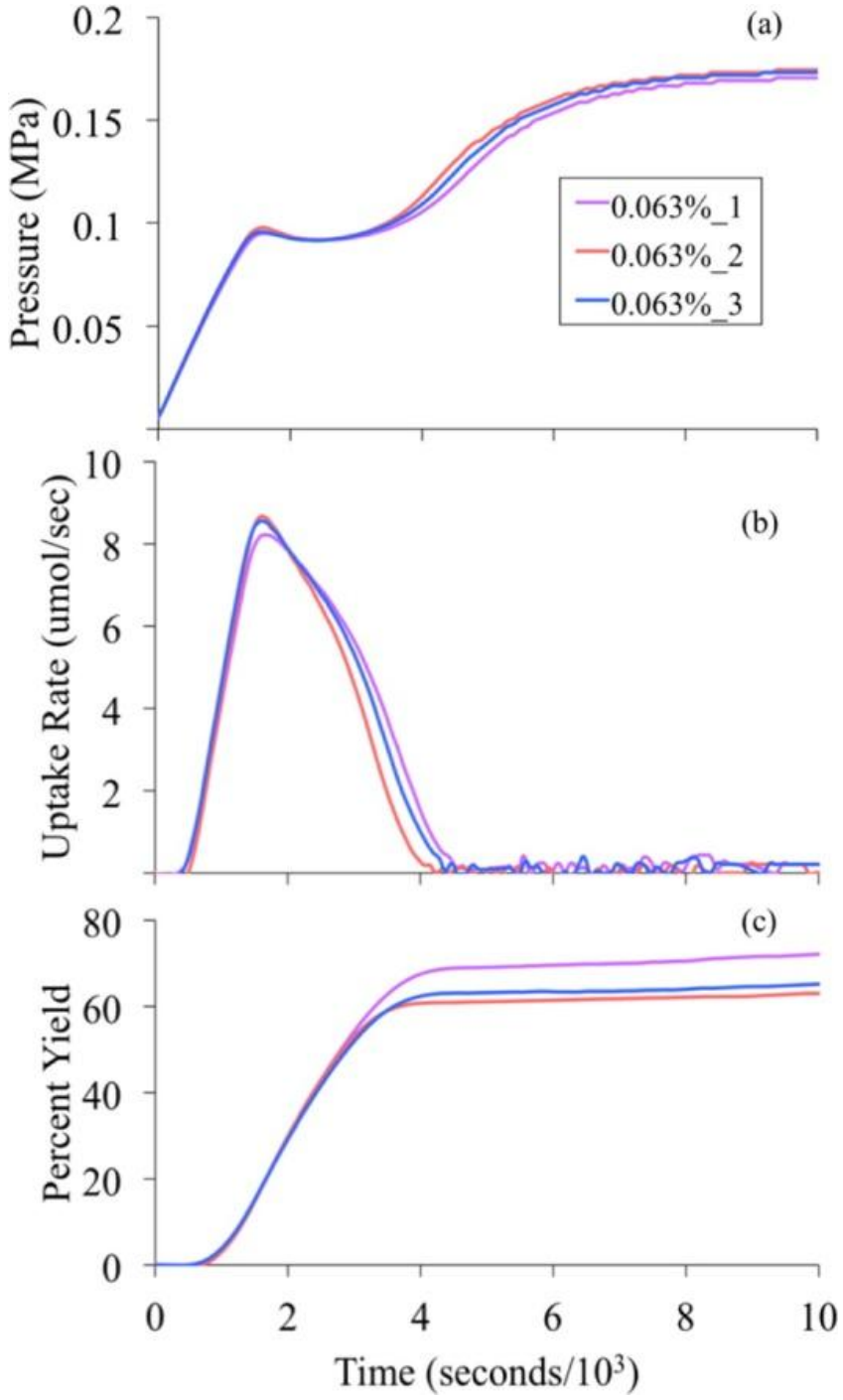

Figure 4: Three experimental runs of 0.063 wt% methanol doping, confirming the reproducibility of the reaction.
(a) Pressure versus time profile . **(b)** Uptake rate versus time. **(c)** Corresponding percent yield versus time.[48]
Reprinted with permission from Reference 48. Copyright (2016) American Chemical Society

The most profound effect discovered in this study is that a small amount of methanol doping can greatly enhance the reaction rate of propane CH formation, especially during the initiation phase, Stage I. In fact, the nucleation of CH formation on the ice surface is dramatically increased by the presence of methanol down to the sub part-per-ten-thousand mole ratio. For the 1.0% methanol sample, the reaction rate continues to be enhanced until over half the ice particle is consumed after the initiation occurs. During Stage II, the cell pressure of the 1% sample is only slightly above the equilibrium vapor pressure of propane CH.[47] In other words, there is no need to have overpressure to drive the CH formation rate to be equal to the gas flow rate into the reaction cell under these conditions. As the formation reaction proceeds, enough methanol remains in the interfacial region between the ice surface and hydrate shell to continue accelerating the reaction rate. In the previous studies, the slow reaction occurring in Stage II is often due to the significantly large coverage of CH on ice surface. As a result, further CH formation is limited by the diffusion rates of water and gas molecules through the CH shell.

In order to test this conclusion, an additional experiment was performed in which pure ice particles were added to the reaction cell filled with liquid nitrogen and followed by adding 0.08g of methanol. Even though the methanol and ice particles were added separately, the overall methanol/water ratio is still similar to that of the 1% methanol doped sample but the difference is that the methanol is initially on the surface of the ice particles at this time. Because the methanol will melt upon heating to 253 K, we assume that the methanol proceeds to physisorb on the ice surface before gas is added to the reaction cell. In this case, there should be a significantly higher surface coverage by the methanol molecules than in the experiments with regular 1.0% methanol doped sample. As expected, the initiation stage of CH formation in this experiment is as fast as we observed in the regular 1.0% methanol doped sample. However, the formation reaction

transitions to Stage III with only about 55% percent yield which is lower than that of the 1.0% sample. This result indicates that there might be more uniform CH shell created on the ice surface from the initial faster reaction which essentially leads to a lower percent yield to the onset of Stage III. Surprisingly, the percent yield of Stage II is still greatly enhanced over that for pure ice samples even when the methanol is added separately. As a result, this experiment suggests that a long-term enhancement of CH formation can still be facilitated by a significant fraction of the methanol added on the ice surface.

In the previous kinetic study of propane CH by Rivera *et al.*, the method of calculating the effective activation energy for Stage II was discussed.[41] Due to the complexity of determining the effective surface area, an instantaneous rate constant $k_{a,T}$ was defined to perform an Arrhenius analysis, where a is the percent conversion up to that point, assuming that for a given percent conversation, the effective surface area is independent of temperature. Thus, the rate of uptake can be expressed as $R = k_{a,T}P_c$, where P_c is the propane pressure. By plotting $\ln(k_{a,T})$ versus 1/T, an activation energy can be extracted from the slope. In their study, a negative activation energy of - 3.8 ± 0.1 kJ/mol (H_2O) was reported for the Stage II reaction which suggests that the rate-limiting step occurs early in the reaction and involves either the sticking of propane onto the surface or the meta-stability of the empty cages in the CS-II propane CH. However, the recent study on difluoromethane CH invalidated the empty-cage hypothesis and they postulated that the strength of adsorption of gas molecules to the ice surface is an alternative origin of the negative activation energy.[42] If there is more concentrated propane at the methanol-water interface compared to the ice surface, the catalytic role of methanol may involve some surface modification processes that facilitates the entry of gas into the ice core shell. In our study, the average activation energy of the initial stage of propane CH formation is -65 ± 1.7 kJ/

mol(C_3H_8) by using the hydration number of 17. If the surface adsorption is the rate-limiting step for the acceleration of reaction, the formation of propane CH from the methanol-water mixture should result in a more negative activation energy. However, not enough evidence from this exists in literature.

At this point, the most important and interesting question from our study so far would be the role of methanol in the accelerated formation reaction of propane CH. With an average molecular diameter of 0.44nm, methanol is supposed to fit well into the large $5^{12}6^2$ cages of a CS-I structure. A recent study confirmed that the CS-I structure can have a full occupancy of methanol in the large $5^{12}6^2$ cages and partial occupancy in the small 5^{12} cages.[38] In the case of CS-II propane CH, if all the small cages are filled with methanol, the water to methanol ratio would be 8.5 with 136 water molecules over 16 cages. Thus, for the highest methanol concentration (1 wt% sample), only 0.1g of methanol occupies the small cages which is relatively insignificant. This also implies that the excess of methanol should not cause phase separation during the initial formation. One may say there is a possibility that methanol acts as a co-guest to participate in the formation of propane CH. However, our study does not focus on methanol-propane double hydrate system and the data analysis is not sensitive enough to allow us to trace down the amount of methanol used in this study. Therefore, we did not take into account the fact that methanol might be incorporated in the empty small cages. More importantly, there is no evidence from the literature to show that the methanol is capable of replacing propane molecules to occupy the large cages only.

To the best of our knowledge, the most similar study of methanol in CH system is by Ripmeester and co-workers on methane doped with ammonia.[34] The methane CH was formed by exposing the gas to the ice particles doped by methanol and ammonia concentration from 0.6 to

10 wt% at an initial pressure of 12.4MPa. However, their experimental method is quite different. The CH formation rate was measured by monitoring the pressure drop in the reaction cell without the continuous gas flow and the size of the ice particles was not reported. Moreover, the reaction was initiated at a large methane overpressure, so any effect on the Stage I nucleation rate was hardly observed. For their study, the initial pressure drop was two orders of magnitude faster for 1.2% methanol doping than pure ice but less for 1.4% ammonia doping. Higher and lower doping resulted in less CH formation enhancement. The authors further concluded that the inhibition effect on CH formation by methanol in oil pipelines must occur before any ice is deposited onto the surface of the pipes.

So far, the current study on propane and the study of methane CH formation discussed above have revealed fascinating phenomenon of CH formation in the presence of small amounts of methanol. However, there are still some open questions needed to be answered regarding its microscopic mechanism. For example: Why does the effective initiation pressure for the reaction drop so dramatically? How does the reaction rate stay so fast as many thousands of monolayers of ice react? Moreover, from the recent study of CF_2H_2 clathrate hydrate formation, due to more uniform coverage of the ice particle surface by CH, higher gas flow rates lead to the faster onset of Stage III kinetics.[42] Conversely, our study shows about 2/3 of the ice is consumed before the onset of Stage III after just over an hour with 1.0% methanol doping. Therefore, many subsequent experiments and simulations will be required to explain the hypotheses made in this study. It would also be interesting to design an experiment capable of measuring the effect of methanol doping on the diffusion limited Stage III regime.

2.3 Conclusion

The experiments clearly show that the methanol doped ice particles have profound enhancement on the propane CH formation rate even with 0.016% methanol concentration. The overpressure required to initiate the reaction drops noticeably; the maximum uptake rate is enhanced; and the reaction rate stays elevated to a higher percent yield before entering the diffusion limited Stage III. The results are compared to a previous study showing that methanol and ammonia dramatically enhance the CH formation rate for methane[34] and also suggest that if CHs are to be used for gas storage, a small fraction of methanol will greatly enhance formation of the hydrate. On the flip side, ice will be quickly converted to CHs in the presence of trace amounts of methanol, and this should be taken into account if methanol is to be used as a thermodynamic inhibitor in gas pipelines. On the other hand, these results, if anything, increase the mystery of how methanol serves as a CH formation inhibitor or catalyst inside of petroleum pipelines.

2.4 Experimental Methods

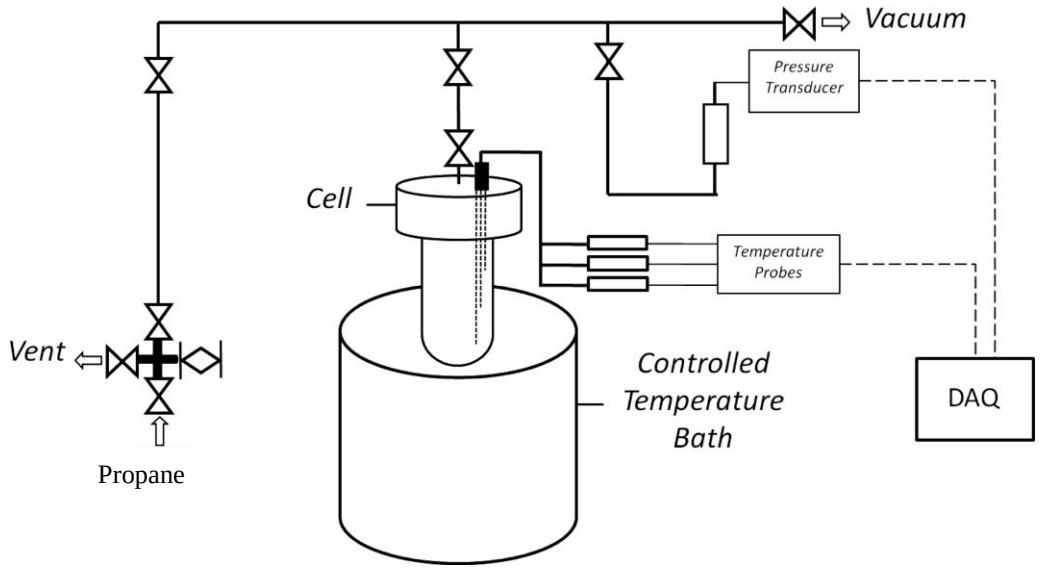

Figure 5. A schematic of the experimental apparatus. Adapted with permission from Reference 42.Copyright (2016) American Chemical Society.

The experiments were conducted in a similar way to the previous kinetic studies of propane and difluoromethane CH formation.[41,42] A series of methanol solutions were prepared by diluting the 1% concentration by a factor of four into 0.016% with nano-pure water. Liquid water containing various amount of methanol was dripped into liquid nitrogen to form frozen methanol-water droplets of roughly 3mm diameter. Then these droplets were ground into fine powder by a coffee grinder in a 253K freezer and size-selected by a sieve with pore diameter of 75 μm under liquid nitrogen temperature. In each experiment, approximately 10g of size-sorted methanol-water powder was loaded into a 310 mL detachable reaction cell precooled with liquid nitrogen, which was later connected to the gas manifold. The temperature of the reaction cell was regulated by submerging it into an ethylene glycol and water mixture bath cooled by a Thermo Neslab RTE 7 programmable refrigeration unit. Then the gas was admitted through a needle valve into the reaction cell to control the flow rate. A fixed pressure was set by a gas regulator to

ensure that the gas pressure was sufficiently high enough for the formation of the hydrate but not exceeding the vapor pressure to be liquefied. The manifold pressure was monitored by an Omega model number PX302-200GV transducer with an accuracy of ±0.25% and the cell temperature was measured by using three Type-T thermocouples (accuracy ± 0.1℃). Temperature and pressure readings were recorded every 100 seconds by a computer-controlled Omega model number OMB DAQ 56 data acquisition module.

Because the gas flow rate was determined by the pressure difference across the needle valve, a calibration was performed by preparing 10mL of fine sand instead of ice as reference runs in the sample cell. Due to the negligible volume differences between the reference runs and the actual experimental runs, this method also simplified the data analysis process with no volume correction needed. The actual amount of size-selected ice powder in the cell was calculated by weighing the leftover liquid water after decomposing the hydrate at the end of the experiment.

CHAPTER 3: Kinetics of Fluoromethane Hydrate Formation with Methanol Doped Ice

3.1 Introduction

Methane hydrate is the predominant naturally occurring hydrate found in offshore continental margins and under the permafrost. It is also a safety hazard for oil industries because of the formation of clathrate plugs in pipelines. Prevention of methane hydrate formation is a costly part of flow assurance and low-concentrations of kinetic or thermodynamic inhibitors such as methanol and ethylene glycol are used to reduce this risk. Even though methanol has been used as a hydrate inhibitor for nearly 70 years, recent studies indicated that low methanol concentration can accelerate methane hydrate formation.[34,35] In the previous chapter, we found that propane CH formation can be greatly accelerated by methanol doped ice particles down to one part per ten thousand water.[48] Moreover, 60% conversion is achieved within only one hour.[48] These unexpected results motivated us to study a series of examples with varying molecular properties to try to isolate other characteristics that may facilitate the faster formation of hydrates.

3.2 Results and Discussion

In this chapter, we study the effect of ice particles doped with low concentration methanol when they are exposed to fluoromethane gas at 248K. Like other fluorocarbon molecules, fluoromethane has some fascinating molecular properties. Researchers have found that fluoromethane hydrate can prevent itself from further decomposing above the thermodynamic melting points, which is also referred to as the "self-preservation" phenomena.[49,50] This “self-preservation” is a kinetic anomaly, where a layer of ice formed on the hydrate surface effectively acts as a barrier to the further escape of guest gas from the hydrate. Even though fluoromethane

clathrate hydrates can be formed under similar pressure and temperature conditions as propane hydrate, the structures are quite different. For propane CHs, it only fits in the larger cages of the CS-II structure, leaving a majority of empty small cages. However, fluoromethane forms CS-I hydrates and the guest fits inside both the large $5^{12}6^2$ cages and the small 5^{12} cages. The composition of fluoromethane CHs has been studied in detail by both spectroscopic and thermodynamic measurements. Uchida *et al.* showed that the cage occupancies between small and large cages of fluorocarbon hydrates are dependent on the solvent accessible surface area (ASA) by Raman spectroscopy.[51] The guest molecules will fully occupy both large $5^{12}6^2$ cages and small 5^{12} cages when the molecular size is smaller than the critical size:1.5 nm^2 ASA. If the molecule ASA is greater than 1.9 nm^2 ASA, it only fits in the large $5^{12}6^2$ cages. Fluoromethane has an intermediate size between 1.5 and 1.9 nm^2 ASA, which means it can be included in both large and small cages of CS-I structure while leaving some empty small cages. From NMR spectroscopy, the cage occupancy ratio of the 5^{12} cage to that of the $5^{12}6^2$ cage was measured to be 0.61(±0.15).[52] This also confirmed the results from Raman spectroscopy indicating the presence of some empty small 5^{12} cages in the structure. However, these results are based on the assumption that all large ($5^{12}6^2$) cages of fluoromethane clathrate hydrate are fully occupied. In order to determine the cage occupancy at equilibrium, the "de Forcrand" method was applied by Anderson to obtain the hydration number of 6.5±0.1 at the lower quadruple point (Q1, where T = 272.5K and P = 0.2442 MPa).[53] With the hydration number, the fraction of small cages to large cages was calculated as 0.54 ± 0.05 indicating the presence of empty cages in the CH structure, which is also consistent with the results from Raman and NMR studies. The kinetics of fluorocarbon hydrates formation have been previously studied by our lab. We recently reported the effect of gas flow rate and temperature for the formation of difluoromethane hydrate.[42] The

flow rate into the reaction cell has profound effects on the formation rate and yield. As one of fluorinated methane hydrates group, it is crucial to further explore the mechanisms of the formation of decomposition of fluoromethane, which may provide some insights on the practical applications of controlling the methane hydrate formation in industry.

Like the prior propane experiments, the results are reported here based on the three-stage shrinking core model as well. In short, fluoromethane gas is leaked through a needle valve into the sample cell where it is exposed to the ice particles at 248K. The pressure inside the sample cell increases monotonically and then decreases even though gas is continuously flowing into the cell which indicates the initiation of the formation. After the reaction enters Stage III kinetics, the pressure slowly rises again. Eventually the cell pressure levels off when it reaches the gas regulator pressure. The clathrate hydrate formation pressure profile as a function of time is shown in **Figure 6 (a)**. Six data sets of reference, ice, and 1 to 0.016 wt% of methanol concentrations are presented respectively. The top yellow curve is the reference run in which 10mL fine sand was used instead of ice. As expected, there is no reaction occurring in the beginning of each trial as the pressure rises monotonically. The red curve is the sample with pure ice. The pressure in the sample cell reaches a threshold ~0.130 MPa where the monotonic increase stops because the gas uptake rate by the particles is greater than the flow rate at this stage. This reaction regime is referred to as Stage I in accordance to the shrinking core model. The pressure profiles of methanol concentrations from 0.016 to 1 wt% in frozen water-methanol mixture are shown in the other four curves. In the lowest methanol concentration (0.016%) sample, the threshold of the initiation pressure drops from 0.130 MPa to 0.110 MPa compared to the pure ice sample. For the highest concentration (1%) sample, the initiation pressure is lowered to 0.090 MPa. Among all methanol-doped samples, the lowest concentration has the highest

initiation pressure and the other two intermediate concentrations 0.063% and 0.25% are slightly higher than the 1% methanol concentration sample. It is very obvious that even with the lowest concentration of methanol (0.016%), the reaction starts at much lower pressure than pure ice. This result agrees well with the previous study of propane.[48] The results are reported in Table 2.

In Stage II, the pressure stays nearly constant after the initial pressure drop of Stage I but the duration varies with the concentration of methanol. During this stage, the reaction rate is almost equal to the gas flow rate. According to the recent propane hydrate study,[48] the surface of most ice particles is covered by hydrate shell but may still be able to have contact with gas molecules. In highest concentration 1% methanol sample, the Stage II pressure is only slightly higher than the vapor pressure of fluoromethane CHs which is about 0.080 MPa at 248K.[53] Similarly, the two intermediate concentration (0.25% and 0.063%) methanol-doped samples have slightly higher Stage II pressure than the vapor pressure. At the lowest concentration (0.016%), the minimum pressure at Stage II remains steady for a while after it drops from 0.110 MPa to 0.090 MPa (**Figure 6 (d)).** It is interesting to note that the duration of Stage II in each run is quite different. The Stage II of the 1% sample only lasts 0.3 hours. In contrast, at the lowest concentration of 0.016% sample, the duration of Stage II is almost about 0.6 hours.

In **Figure 6 (a)**, the pressure profile seems to have the trend that the lower the concentration is, the longer the Stage II lasts. In this study, the gas is set at much higher flow rate than the previous kinetic study of propane CH with methanol.[48] The effect of gas flow rate on the growth kinetics of difluoromethane CH was that a fast flow rate usually results in a faster initial reaction rate in the Stage I regime and also stops the CH formation much sooner than a slower flow rate experiment.[42] In this current work, the monotonic increase of initial pressure stops at 15 minutes and the Stage II of all samples generally lasts about 1.25 hours. These results are relatively

consistent with the results from the difluoromethane study.[42] However, the pressure profiles indicate that the surface coverage seems to depend on the concentration of the methanol. The duration of Stage II in the highest concentration (1%) sample lasts about 20 minutes, which is almost half of the duration of Stage II kinetics in the 0.063% sample. The hypothesis made by Amtawong *et al.* that a fast flow rate forms more uniform ice coverage, which obstructs the further contact and reactions between gas molecules and ice particles still holds.[48]

As the reaction proceeds further, the coverage of ice particles is sufficient to limit the exposure to the fluoromethane gas molecules. The slow diffusion of fluoromethane through the hydrate layer governs the reaction regime which leads to the pressure gradually approaching the final pressure of the reference run, which is indicative of Stage III kinetics. Since this slow diffusion-dominant Stage III cannot be recorded precisely by the current techniques, we stop the experiment before the full completion of Stage III. Again, the definition of the three reaction stages is empirical, in analogy with the shrinking core model.

Table 2. Data of the Growth Kinetics of Fluoromethane Clathrate Hydrate

Methanol Concentration (wt %)	Mass of Ice (g)	Initiation Pressure (MPa)	Maximum Uptake Rate (μmol/s)	% Conversion	Duration of State I and II ($s/10^3$)
0 (pure ice)	9.4	0.130	11.4	60	2.7
0.016	10.1	0.110	9.6	65	2.8
0.063	10.6	0.100	8.0	66	3.0
0.25	10.9	0.091	7.8	53	1.9
1.0	10.5	0.090	7.5	65	1.7

By applying the Peng-Robinson equation, the uptake rate of gas into fluoromethane clathrate hydrate at any instant can be derived and calculated from the formulas below:

$$PV = ZnRT \qquad (1)$$

$$\frac{dn_m}{dt} = \frac{dn_{cell}}{dt} - \frac{dn_{clathrate}}{dt} \qquad (2)$$

where V is the volume of the reaction cell occupied by fluoromethane, Z is the compressibility factor as a function of pressure and temperature, P is the pressure of the gas inside the reaction cell which can be converted into the number of moles n. R is the ideal gas constant, and T is the average temperature. $\frac{dn_m}{dt}$ is the rate of change of the moles of propane calculated from the measured pressure change for an experimental run, $\frac{dn_{cell}}{dt}$ is the flow rate of the propane gas into the cell calculated from a reference run, and $\frac{dn_{clathrate}}{dt}$ is the uptake rate of propane into clathrate.

Figure 6 (b) is the uptake rate profile versus time. The maximum uptake rate is notably large in the pure ice sample. It is interesting that the lowest concentration sample (0.016%) has a similar uptake rate profile. A rapid drop occurs after reaching the peak of the uptake rate, followed by a flat shoulder regime lasting until $3x10^3$ s. For the other samples, there is no "overshoot" on the uptake rate curves. A flat region immediately occurs after the initial monotonic increase. In the previous paper, we attributed the negative slope region of the uptake rate curves to Stage II of formation, and the positive slope region with the peak of uptake rate to Stage I. In this study, the data indicates that the lower concentration samples seem to gather higher fractions of fluoromethane molecules near the ice surface than the higher methanol concentration samples at the same reaction time. The initial rise of the maximum uptake rate is due to a fast formation of the hydrate layer from the encounter between gas and ice particles. In the flat shoulder regions, the reaction rate slows down due to the effect of gas adsorption to the

ice surface. After the initial fast creation of the hydrate layer, most of the ice particle surface is covered. The rate of gas molecules entering the ice surface is slightly higher than the number of the available reaction sites, which results in a gradual decrease in reaction rate subsequently. As more and more reaction sites are converted into hydrate, the reaction dramatically slows down regardless of the methanol doping during the onset of Stage III.

By integrating the uptake rate curve over time, the total amount of fluoromethane can be determined. The percent yield is then calculated by using the hydration number of 6.5 that was estimated by Anderson.[53] The percent yield versus time curves are presented in **Figure 6 (c)**. For the methanol doped samples, the percent yield is higher with decreased methanol concentrations. For example, the percent conversion for 0.016% is about 65% and that for 1% is about 57%. When the percent yield curves level off, Stage III of formation has reached : 1.6 x 10^3 s for 1%, 1.9 x 10^3 s for 0.25%, 2.6 x 10^3 s for pure ice, 2.8 x 10^3 s for 0.016%, and 2.9 x 10^3 s for 0.063%.

The experiments were repeated to verify the reproducibility of the measurements. **Figure 7** demonstrates three runs for the 1% methanol doped sample. For the pressure profiles, the initiation pressures of three runs are all ~0.09 MPa. The maximum uptake rate ranges from 7.4 to 7.7 μmol/sec and the percent yield ranges from 66% to 73%. The main variation observed may be the duration of Stage II in the pressure profile that is from 0.75x10^3 s to 0.9x10^3 s. This also reflects to the uptake rate profile that the flat shoulder regions of three runs are slightly different which affects the overall percent yield. Despite the simplicity of our experimental techniques, especially the production of ice particles and the size sorting, all three data sets are very similar and we conclude our results are well reproducible. Repeated experiments were also conducted for the other concentration samples and the results are quite satisfying.

In contrast to the previous methanol-doped propane experiment, we do not observe any evidence that an addition of small amounts of methanol accelerates the hydrate formation rate. Although doping with even less than one part per then thousand mole ratio concentration lowers the initiation pressure. All methanol-doped samples have lower initiation pressures than the pure ice sample and the 1% sample indeed has the lowest initiation pressure. However, despite the reduction in the initiation pressure, the maximum uptake rates are showing opposite results compared to the propane study. In the propane experiment, the highest maximum uptake rate was found in the 1% sample. All the other methanol-doped samples have much higher maximum uptake rates than the pure ice. In the current fluoromethane experiment, the pure ice sample has the highest maximum uptake rate compared to all the methanol doped samples. It seems that the lower concentration samples have higher maximum uptake rates. This indicates that the methanol does not catalyze fluoromethane hydrate formation. In fact, it seems to have a slight inhibitory effect. Furthermore, the duration of the Stage II reaction has an inverse dependence on the methanol doping concentration. The lowest doping concentrations (0.016% and 0.064%) have a slightly longer Stage II reaction time than pure ice. But for the highest methanol concentrations (1% and 0.25%), the duration of Stage II is significantly shorter than that of pure ice. We suspect that the slightly longer Stage II duration for the lowest methanol concentrations is due to the injection of defect structures, as theorized by the Trout-Buch mechanism.[54–56] However, at the higher concentrations of methanol, the inhibitory effect of the methanol negates any advantages derived from the better diffusion of gas molecules through the ice due to the injection of defects. We postulate that as the reaction proceeds, the amount of methanol molecules in the interfacial region determines the surface hydrate layer formation. For the highest concentration sample (1%), the outer hydrate shell formation is accelerated by the large

population of methanol molecules. As the hydrate layer quickly builds up, the outer shell is thick enough that it can significantly hinder the entry of fluoromethane gas molecules into the ice particles. Consequently, the duration of Stage II is eventually shortened.

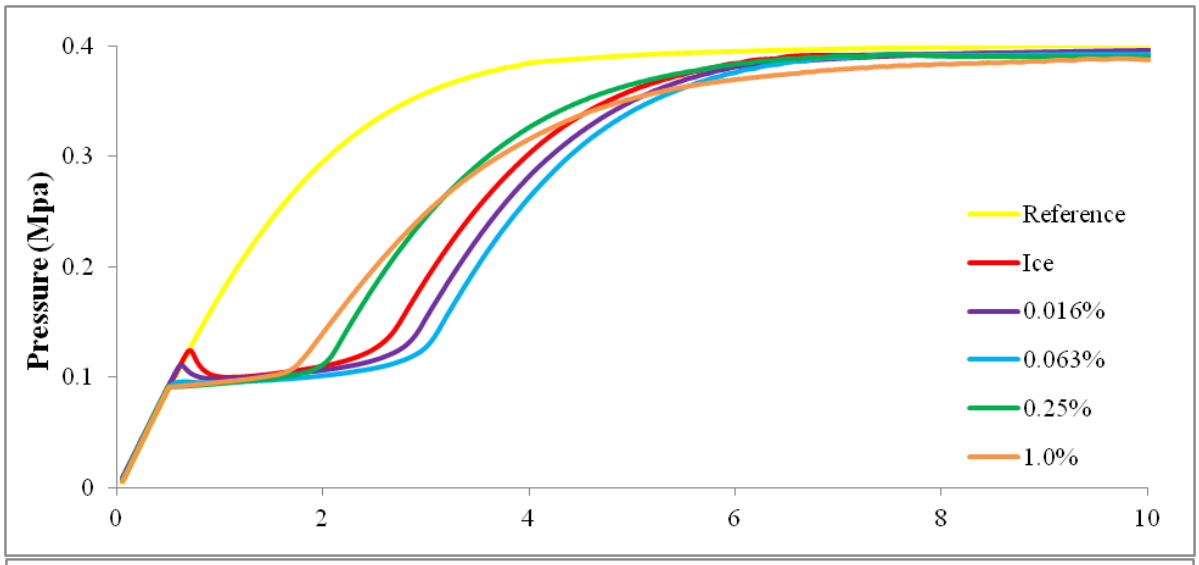
Pressure (Mpa)
0.4
0.3
0.2
0.1
0
0
2
4
6
8
10
Reference
Ice
0.016%
0.063%
0.25%
1.0%

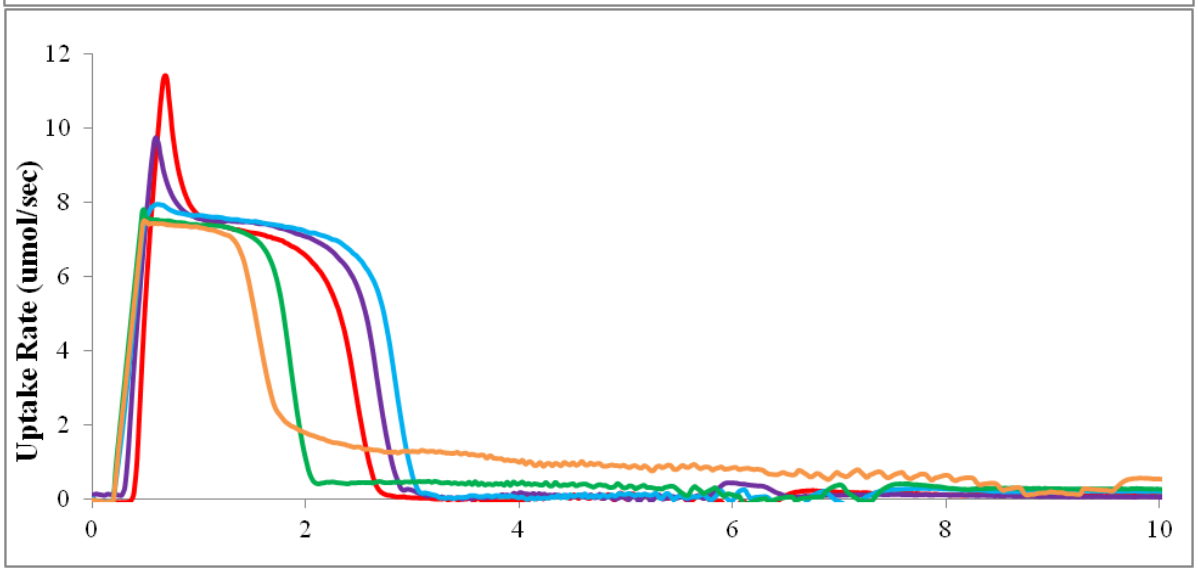
Uptake Rate (umol/sec)
12
10
8
6
4
2
0
0
2
4
6
8
10

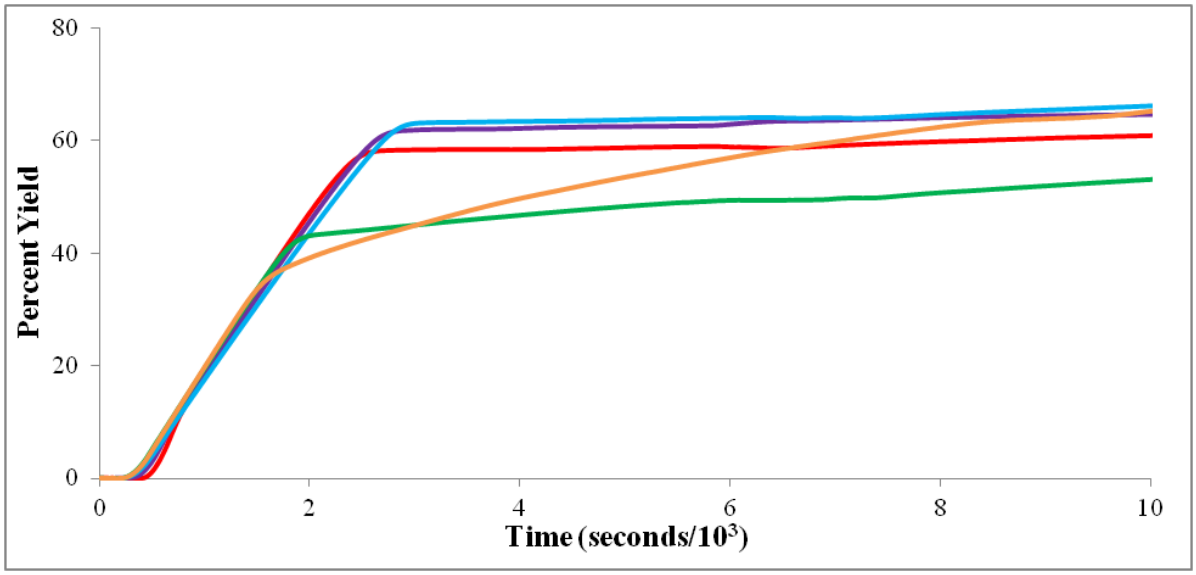
Percent Yield
80
60
40
20
0
0
2
4
6
8
10
Time (seconds/10³)

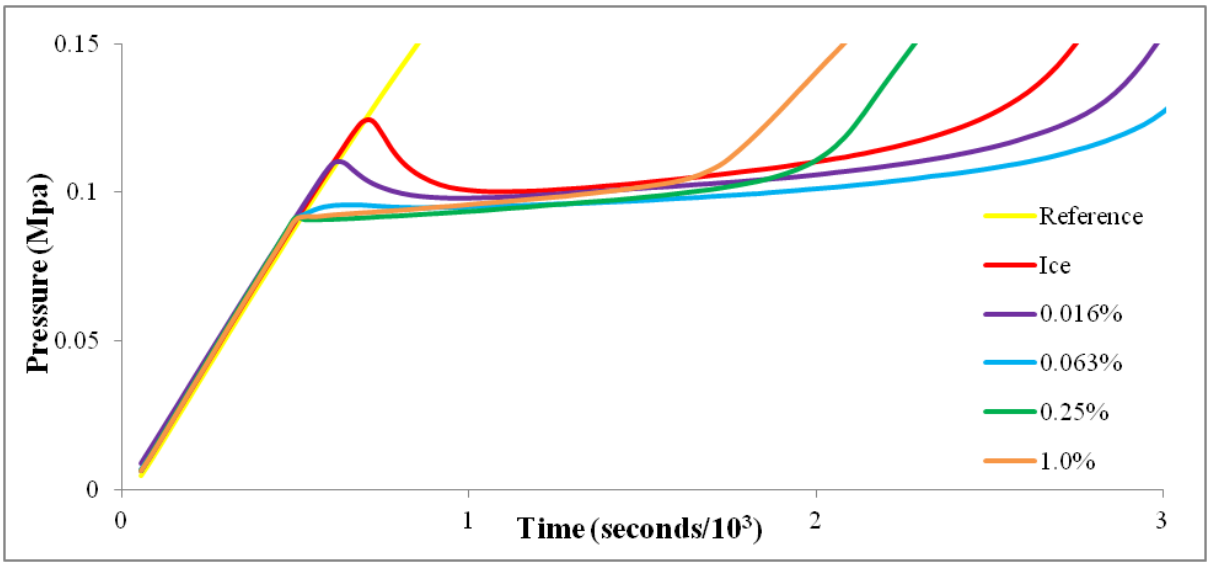

Figure 6:
(a) Pressure versus time profile of a reference run, a pure ice sample, and 4 experimental runs of methanol doped ice concentrations at 253K.
(b) Uptake rate versus time.
(c) Percent yield profile.
(d) A zoom-in view of initiation pressure.

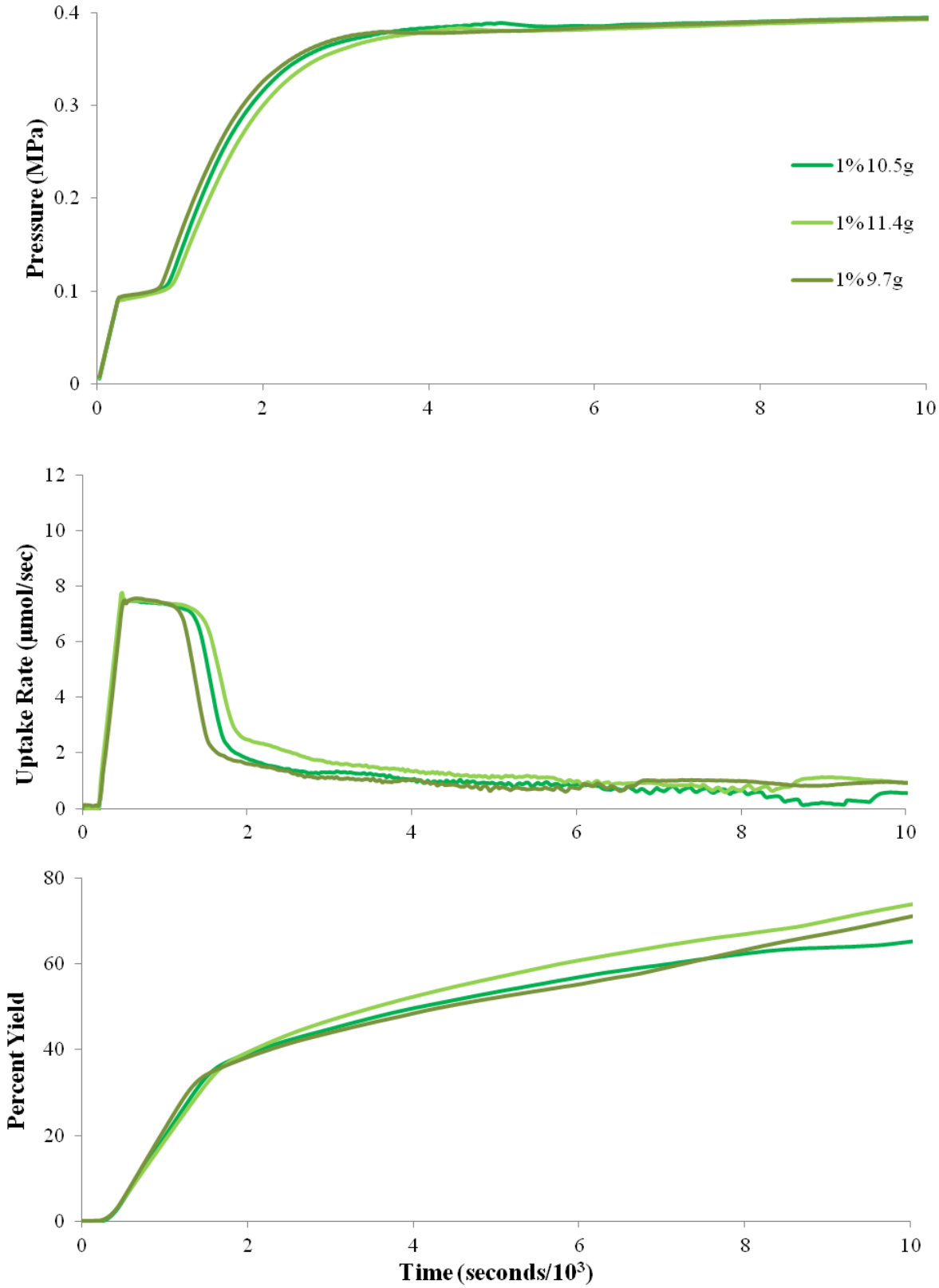

Figure 7: Three experimental runs of 1 wt% methanol doping, confirming the reproducibility of the reaction.
(a) Pressure versus time profile . **(b)** Uptake rate versus time. **(c)** Corresponding percent yield versus time.

3.3 Conclusion

This study is the second experiment investigating the catalytic effects of methanol on the series of CH formation. Our previous paper on propane hydrate formation concluded that the presence of a small amount of methanol in the interfacial region may accelerate the fluoromethane CH formation by facilitating the adsorption of propane gas to the ice surface.[48] In the current work, we observe that while this might be true, it does not fully account for the catalytic effect. The initiation pressure for the fluoromethane hydrate formation does decrease with the increase of methanol concentration, indicating that methanol increases the chances of the gas interacting with the ice surface. However, this reduction in initiation pressure is not accompanied by an increase in the peak uptake rate. In fact, the peak uptake rate is decreased with increasing methanol concentration. We also observe that the duration of Stage II is dependent on the methanol doping concentration. The higher concentration samples tend to stall the reaction sooner and thus have shorter Stage II duration. Therefore, in our opinion, the catalytic activity of methanol is dependent on the nature of the guest gas itself. It should be noted that propane and methane are non-polar molecules, while fluoromethane is a polar molecule. The interaction of the gas molecules with the methanol and with the quasi-liquid layer (QLL) on the ice surface are different. The QLL has been shown to be essential in the formation of clathrate hydrates on the surface of ice.[57,58] It is possible that methanol doping increases the QLL present on ice surface, and thereby facilitates the initiation of the reaction, leading to a decrease in the initiation pressure for all the gases. However, the more polar fluoromethane molecules might prefer to concentrate in the QLL and thereby participate mostly in the reaction on the ice surface. We postulate that, as the reaction proceeds further, the build-up of the outer shell in the high methanol concentration samples occurs faster and therefore is thicker than the lower methanol

samples. The surface of ice particles is more quickly and uniformly covered and consequently hinders the fluoromethane gas molecules from entering the inner layers of ice, even though the diffusion process itself might still be helped by defects.

3.4 Experimental Methods

The schematic of this experiment and the procedure used in the present work are similar to those used in the previous experiments on propane clathrate hydrate formation with methanol doped water.[48] Ice particles were prepared by dripping the methanol + water solution with various concentrations into liquid nitrogen and ground into ice powder using a coffee grinder in a 253K freezer afterwards. Then the ice powder was size-sorted by a 75μm sieve under liquid nitrogen temperature. For each concentration, approximately 10g of size-selected ice particles were transferred into a 310mL reaction cell precooled with liquid nitrogen which was then quickly connected to the gas line. Meanwhile, the reaction cell was submerged into a chilled mixture of ethylene glycol and water bath at 248K controlled by the Neslab RTE 7 programmable refrigeration unit. The fluoromethane gas pressure was preset by a gas regulator to 0.41 MPa (60 Psi), so the gas pressure was lower than the vapor pressure of fluoromethane to avoid any liquid formation but high enough for the formation of fluoromethane CH. When the reaction cell reached the temperature of 248K, fluoromethane gas was admitted into the reaction cell, and the flow rate was controlled through a needle valve. Fluoromethane was purchased from Airgas with a stated purity greater than 99%.

The calibration step is also similar to the propane/methanol experiment in that a reference run was performed with 10 mL of fine sand in the sample cell in lieu of ice to calculate the gas flow rate into the reaction cell. The actual mass of ice particle consumed in each run was determined

by weighing the water left behind after the decomposition of the hydrate after each experiment and this mass was used in the calculations for the data analysis process.

CHAPTER 4: Dynamic Study on Guest-Cage Interactions in Clathrate Hydrate

4.1 Introduction to NMR

An important quest of physical chemistry is to concisely understand the structure and chemical properties in the molecular level. In the field of clathrate hydrate, NMR has long been employed as a suitable tool to investigate their composition and formation kinetics. In this project, solid-state NMR will be used to explore the guest-host interactions in the hydrate system which can potentially expand the current understanding of the structure and dynamics of clathrate hydrates. Therefore, a brief introduction to NMR theory is presented here to aid in the understanding of the rest of the thesis.

Nuclear Magnetic Resonance spectroscopy has been developed into a powerful tool with a vast range of applications from molecular structure determination to synthetic products characterization, chemical analysis, and dynamic study of physical and biological systems. The non-invasive and non-destructive nature of NMR is a very important advantage over other methods (such as neutron diffraction) for characterizing molecules. Thus, it is widely used to distinguish structures including relative configurations, and even closely related species that differ in intermolecular interactions.

In the early 1920s, the measurements of electron spin and the magnetic moment of the electron were widely established. Stern and Gerlach successfully separated beams of atoms by using an inhomogeneous magnetic field according to the orientation of the electron magnetic moment.[59] Sooner, in 1939 a major improvement was made by Rabi *et al.* to deflect a beam of hydrogen molecules though a homogeneous magnetic field.[60] The small but measureable deflection of the beam was caused by the energy absorbed by the molecules at a characteristic

radio frequency. This work was credited as the first observation of NMR and the method could be used to determine the magnetic moments of nuclei. In 1940s, a significant achievement was made by Felix Bloch and Edward Purcell independently.[61,62] Bloch found that the nuclear magnetization could be rotated away from its equilibrium position by applying a certain RF frequency. The displaced magnetization would precess about the magnetic field and essentially induce an electrical signal which was detected by a perpendicular receiver coil.[61] Almost at the same time, Purcell observed the small absorption of RF energy by the proton magnetic moments in a block of paraffin.[62] Later, they were jointly awarded the Nobel Prize for physics in 1953 for this discovery. In the early days of NMR, design and construction of a sufficiently homogeneous and stable magnet to detect reasonably NMR signals by electronic circuits were the major tasks for scientists. Fortunately, after the first commercial NMR system was produced by Russell Varian, the development of stronger superconducting magnets and pulsed Fourier Transform (FT) NMR had rapidly led the NMR techniques toward its advanced modern era.[63] With sufficiently high magnetic fields, researches could spread out the spectrum and distinguish chemical shifts in large molecules that might nearly be coincident at lower magnetic fields. In FT NMR, the spins of nuclei were first allowed to equilibrate with a static polarizing magnetic field B_0, and then an oscillating magnetic field B_1 using a radio frequency (RF) pulse brought the spins out of equilibrium. The time-dependent precession of the spins was detected and transformed by FT from the time domain to frequency domain. This revolutionized method did not only shorten the data acquisition time but also provide possibilities to exploit the fast processes of chemical reactions, multidimensional spectroscopy for biological samples, and time-dependent NMR phenomena.[64]

Although most NMR experiments are performed in liquids in which narrow lineshapes achieved by averaging the anisotropic interactions from free tumbling, a wide range of additional interactions are still present in the solid phase. Solid-state NMR spectroscopy has been developed rapidly and is being used to quantitatively determine the molecular structure, conformation and dynamics of a variety of solid systems including liquid crystals, gels, proteins, and polymers. This chapter is intended to introduce the fundamental theory and concepts of NMR spectroscopy.[65–67]

4.1.1 Basic Theory of NMR

When nuclear spins are placed in an external magnetic field, they will align along the field and also generate small magnetic dipole. The magnitude of the spin-angular momentum $\hbar\mathbf{I}$ is given by

$$\hbar|\mathbf{I}| = \hbar[\mathbf{I}\cdot\mathbf{I}]^{1/2} = \hbar[I(I+1)]^{1/2}$$

where I is the spin-angular quantum number. In order to be "NMR active", an element must have a non-zero spin-angular quantum number. For the nuclei with even mass number and even atomic number, the total spin quantum number, I will be 0, which is NMR inactive. On the other hand, if nuclei have an odd mass number, the spin-angular quantum numbers will be half-integer, and nuclei with even mass number and odd atomic number have integer spin-angular momentum quantum numbers.

In Cartesian coordinates, the z component of spin-angular momentum is written as,

$$\hbar I_z = m\hbar$$

where m is the magnetic quantum number. For a given I, m takes value from +I, -I+1,..., I-1, I with total 2I+1 states.

In a non-zero spin-angular momentum, the magnetic moment (μ) is expressed as,

$$\mu = \gamma \hbar I ,$$

where γ is a characteristic constant of the nucleus called the gyromagnetic ratio with the units of $(T\ s)^{-1}$.

When an external magnetic field is applied, the energy is given by,

$$E = -\mu \cdot B$$

where B is the magnetic field vector. In conventional NMR, the external static magnetic field is along the z-axis of the laboratory coordinate system. Therefore, this equation can be reduced to the z-component only,

$$E = -\mu_z B_z = -\gamma \hbar I_z B_0$$

where B_0 is the strength of the applied external magnetic field. For a spin I under the influence of a fixed magnetic field, the energy levels split into (2I+1) sublevels and the energy difference between neighboring levels can be expressed as

$$\Delta E = \gamma \hbar B_0$$

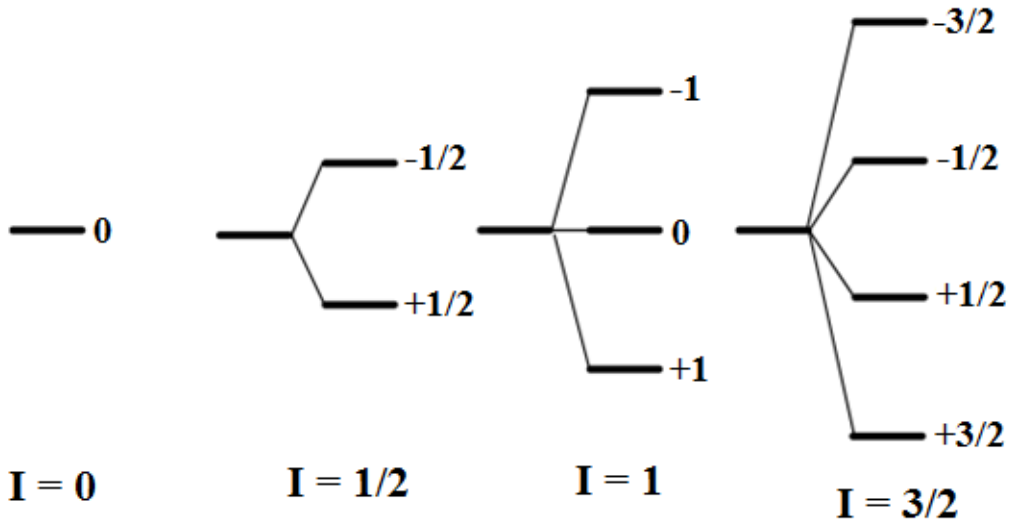

Figure 8. The energy level splits into (2I+1) levels under the influence of a magnetic field.

These 2I+1 energy states are referred to as Zeeman states and the energy levels are displaced by a constant value, $\gamma\hbar$ B_0, which generally can be expressed in terms of a characteristic frequency, the Larmor frequency. As Larmor frequency is directly proportional to the applied field, the **Figure 9** shows, the larger the magnetic field, the higher resonance frequency.

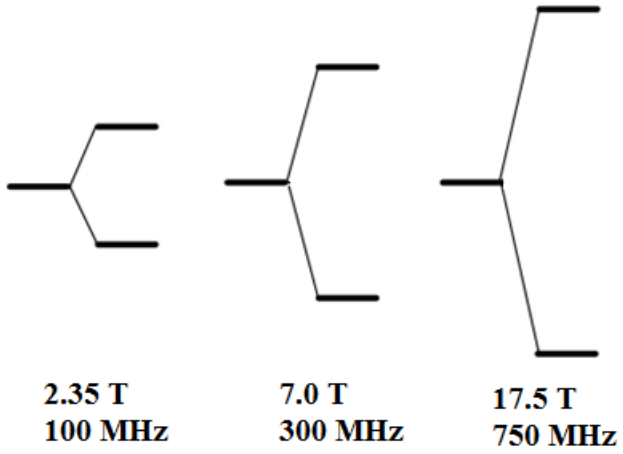

Figure 9. The energy difference between two adjacent levels depends on the strength of applied magnetic field B_0.

4.1.2 Solid-State NMR

Most conventional NMR experiments are conducted in liquid samples where molecules can randomly tumble around at a fast rate. Well-resolved and narrow lineshapes can be easily achieved due to the averaging of the anisotropic interactions. Unlike in the liquid phase, there is a wide range of additional interactions in the solid phase including chemical shift anisotropy, dipole-dipole coupling, and quadrupole couplings.

For a two-spin system I and S in solid phase, the dipolar coupling arises from an interaction between the magnetic moments of two different nuclear spins. In the presence of an external magnetic field B_o, the energy of the spin I and S under the influence of B_o can be described as Zeeman energy,

$$E_{Zeeman} = - \gamma \hbar B_o m_{I/S}$$

where, γ is the gyromagnetic ratio, B_o is external magnetic field strength, and $m_{I/S}$ is spin quantum number for I and S. In the B_o field, each spin has a magnetic dipole associated with it. Furthermore, each spin experiences the field that is generated by the other, thus this interaction is called dipole-dipole coupling or dipolar coupling. The strength of the heteronuclear dipolar coupling is governed by the Hamiltonian,

$$H_{IS} = -d(3\cos^2\theta - 1)I_z S_z$$

where d is the dipolar coupling constant, which is inversely proportional to the cube of the internuclear distance r_{IS} ($\frac{1}{r_{IS}^3}$). The angle θ is the orientation of the internuclear vector with respect to the external field B_o, and I_z and S_z are nuclear spin angular momentum operators of I and S in the z direction. From the equation above, one can tell that the dipolar coupling is a through-space interaction due to the internuclear r_{IS}dependence. It also depends on orientation because of the presence of $(3\cos^2\theta - 1)$ term in the Hamiltonian. This explains why there are no dipolar coupling interactions in liquid samples because the fast tumbling of molecules averages the $(3\cos^2\theta - 1)$ term to zero. In a powdered solid sample, the individual crystallites are oriented in all possible directions and the signal represented for all directions will appear at different resonance frequencies, which will lead to broad and overlapping spectral lineshapes.[66,67]

Chemical shift anisotropy is another important interaction in the solid state. When an external magnetic field is applied to an atom, not only do the nuclear spins experience the field and have magnetic moment, but the electron cloud around the nuclear is also perturbed. The magnetic moment from surrounding electrons create induced circulating currents which also generate a small magnetic field B_e as

$$B_e = -\sigma B_o$$

where, σ is the chemical shift tensor, which is expressed in the lab frame as

$$\sigma = \begin{pmatrix} \sigma_{xx} & \sigma_{xy} & \sigma_{xz} \\ \sigma_{yx} & \sigma_{yy} & \sigma_{yz} \\ \sigma_{zx} & \sigma_{zy} & \sigma_{zz} \end{pmatrix}$$

and the Hamiltonian of the chemical shift is:

$$H_{cs} = \gamma I^T \sigma B_o = \gamma(I_x\sigma_{xz} + I_y\sigma_{yz} + I_z\sigma_{zz})B_o$$

The nucleus feels the induced field as a small perturbation to the external field, so only the local field contribution to the laboratory frame Hamiltonian is retained in the secular approximation. Therefore, the effective nuclear spin Hamiltonian is given by

$$H_o + H_{cs} = \omega_o (1-\sigma_{zz})I_z = \omega_o I_z - \omega_o \sigma_{zz} I_z$$

The second term $\omega_{cs} = -\omega_o \sigma_{zz}$ is also called chemical shielding. In NMR convention, the chemical shielding tensor is often defined relative to the isotropic shielding σ_{iso}, a simple average of the diagonal elements of the shielding tensor. Alternatively the chemical shift frequency can be expressed as:

$$\omega_{cs} = \omega_o \left[\sigma_{iso} + \frac{1}{2}\Delta\sigma(3\cos^2\theta - 1 - \eta\sin^2\theta\cos(2\phi)\right]$$

in which, $\sigma_{iso} = \frac{1}{3}(\sigma_{xx}^{PAS} + \sigma_{yy}^{PAS} + \sigma_{zz}^{PAS})$, anisotropy factor $\Delta\sigma = \sigma_{zz}^{PAS} - \sigma_{iso}$, and asymmetry parameter $\eta = \frac{1}{\Delta\sigma}(\sigma_{yy}^{PAS} - \sigma_{xx}^{PAS})$.

Since all molecular orientations are present in a powdered solid sample, all values of the angle θ are possible. Each different orientation with respect to the applied external field B_o has a different chemical shift associated with it. Therefore, the spectrum will appear as a broad peak covering a range of frequencies due to the different molecular orientations, as a result all lines from the different orientations overlap and form a continuous lineshape. This is also referred to as the powder pattern, which is a rich source of information that can be used to quantitatively determine the molecular structure and dynamics. However, by maintaining all these anisotropic

interactions, the static NMR spectrum appears as a very broad peak. The loss in resolution makes it difficult to study all but the simplest of molecules. Several techniques have been developed in solid-state NMR that can selectively switch on and off these anisotropic interactions in solid samples, thereby retaining the resolution inherent in liquid-state NMR, while still being able to access the structural and dynamical information available from solid-state NMR.

The most common technique to achieve high resolution solid-state NMR spectra with resolution comparable to liquid-state NMR is Magic Angle Spinning (MAS), which was first introduced by E.R. Andrew and I.J. Lowe in late 1950s.[68,69] This technique involves rotating the sample about an axis oriented at $\theta_{\mathrm{M}} = \cos^{-1}\left(1/\sqrt{3}\right) \approx 54.7^{\mathrm{o}}$ with respect to the external magnetic field. Since the two major anisotropic interactions, the dipolar coupling and the chemical shift anisotropy, both contain the $(3\cos^2\theta - 1)$ term, the orientation dependences are averaged out when the sample is spun at $\theta = 54.7^{\mathrm{o}}$.

4.1.3 Relaxation

After a sample is placed in a magnetic field B_0, the equilibrium state is established when a Boltzmann distribution of spins occurs between the energy levels. The processes by which the spins attain an equilibrium distribution of population are collectively called relaxation processes.[70] In NMR, relaxation is actually due to the coupling of the spin system to the surroundings. Historically, the surroundings have been referred as the lattice because the early studies of NMR relaxation were in solids where the surroundings were genuinely a solid lattice. Classically the lattice is assumed to have an infinite heat capacity and consequently to be in thermal equilibrium at all times. The lattice weakly couples the spin system and also modifies the local magnetic fields at the nuclei of interest with random fluctuations, which drives the

relaxation process. Therefore, the total Hamiltonian of the system including the local fluctuating fields can be expressed as

$$H_{Total} = H_{system} + H_{local}(t)$$

where the time-dependent Hamiltonian of local field can be written as

$$H_{local}(t) = -\mu \cdot B_{local}$$

For the locally fluctuating field B_{local}, there are two components, longitudinal and transverse. The longitudinal components are responsible for adiabatic processes. When the fluctuating field is parallel to the static magnetic field B_0, it generates various fluctuations along the B_0 axis that also change the energies in the nuclear spin energy levels. As a result, it randomly varies the energy levels and eventually the phase coherence is destroyed. However, the populations of the states are not changed and no energy exchange occurs between the spin system and the lattice. Transverse components describe a non-adiabatic process of relaxation. Energy is exchanged between the spins and the lattice that brings the spin system into thermal equilibrium with the lattice populations of the stationary state return to the Boltzmann distribution. Moreover, the population of states subject to the condition that the fluctuations have associated frequencies which match the frequencies of transitions for the spins.[70]

In the classical view of NMR, relaxation is the process by which the spins in the sample come to equilibrium with the surroundings. If an oscillating field B_1 perpendicular to the B_0 axis is applied to manipulate the spin system, two different mechanisms describe how spins return to the equilibrium state. T_1 and T_2 are two standard measurements in NMR which are also referred to as spin-lattice or longitudinal relaxation and spin-spin or transverse relaxation respectively. Spin-lattice relaxation describes the return of the longitudinal magnetization to thermal equilibrium

and the spin-spin relaxation describes the decay of the transverse magnetization to zero.[66,67,70] These phenomena are characterized by the Bloch equations:[61]

$$\begin{aligned}
\frac{dM_z(t)}{dt} &= \gamma\left(\mathbf{M}(t)\times\mathbf{B}(t)\right)_z - R_1\left(M_z(t)-M_0\right) \\
&= \gamma\left(M_x(t)B_y(t)-M_y(t)B_x(t)\right)-R_1\left(M_z(t)-M_0\right), \\
\frac{dM_x(t)}{dt} &= \gamma\left(\mathbf{M}(t)\times\mathbf{B}(t)\right)_x - R_2M_x(t) \\
&= \gamma\left(M_y(t)B_z(t)-M_z(t)B_y(t)\right)-R_2M_x(t)\ , \\
\frac{dM_y(t)}{dt} &= \gamma\left(\mathbf{M}(t)\times\mathbf{B}(t)\right)_y - R_2M_y(t) \\
&= \gamma\left(M_z(t)B_x(t)-M_x(t)B_z(t)\right)-R_2M_y(t)\ .
\end{aligned}$$

in which, M(t) is the nuclear magnetization vector with components of $M_x(t)$, $M_y(t)$, and $M_z(t)$ and B(t) is the applied magnetic field including the static and RF fields. R_1 and R_2 are the spin-lattice and spin-spin relaxation rates and they are the inverse of corresponding T_1 and T_2 relaxation times. The rate of relaxation is influenced by the physical properties of the sample, which determine how fast an experiment can be repeated. Therefore, it is important to understand how relaxation rates can be measured and the factors that influence their values.

The Bloch equations provide rich information about the effects from relaxation on NMR experiments which make it possible to experimentally measure these rate constants. For instance, the Free Induction Decay (FID) of the spins can be predicted as the sum of exponentially damped sinusoidal functions with R_1 determining how long it requires for the spin system return to the equilibrium state and R_2 determining the length of time that the FID can be observed.

The spin-lattice relaxation time T_1 is usually measured by the inversion-recovery pulse sequence. The first 180 ° pulse inverts the equilibrium magnetization to the -z axis. Then a delay τ is left for the magnetization to relax back. Following the delay τ, a 90° pulse is applied to rotate the magnetization onto the +y axis where the signal is detected. Note that this is in contrast to the

case for the simplest NMR experiment where the magnetization starts out along +z and it is rotated onto -y.

If the delay τ is set to be a very short time, the magnetization has not changed at the end of the delay. As τ gets longer, there is more time for more relaxation to take place. With sufficient time, the magnetization will shrink towards zero, which results in a negative peak in the spectrum but with decreased magnitude. Eventually the magnetization goes through zero and then starts to increase along +z. This gives a positive peak in the spectrum. Thus, by varying the delay τ, the recovery of the z-magnetization can be mapped out from the intensity of the observed spectra. The whole process is visualized in **Figure 10**.

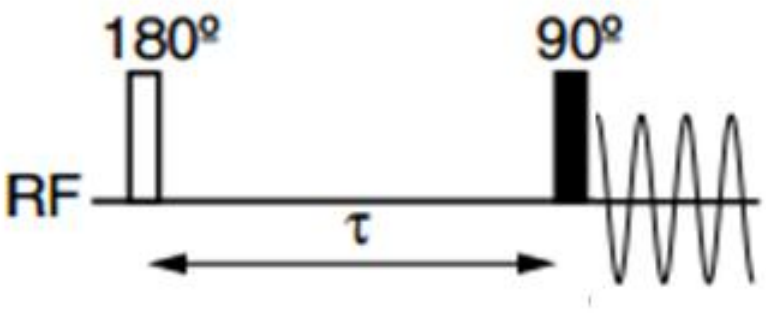

Figure 10. The pulse sequence of Inversion Recovery to measure T_1 relaxation.

The spin-spin relaxation T_2 is usually measured by Spin Echo or "Hahn Echo", which was discovered by Erwin Hahn in 1950.[71] The outcome of the "Echo" is the offset has been refocused; at the end of the sequence it is just as if the offset had been zero and hence there had been no evolution of the magnetization. After the first 90 ° excitation pulse, all the spins start to dephase immediately in the transverse plane as some precess faster and some slower than the average during the delay τ. The following refocusing 180 ° pulse is applied to "flip" all the spins in the transverse plane. As the spin phases are reversed, the faster spins are where the slower ones used to be. Eventually the faster and slower spins rephase as the precession continues and

the time τ for rephasing is equal to the original dephasing time. The echo is formed. Then the T_2 can be determined from the exponential decay of the magnetization in transverse plane.

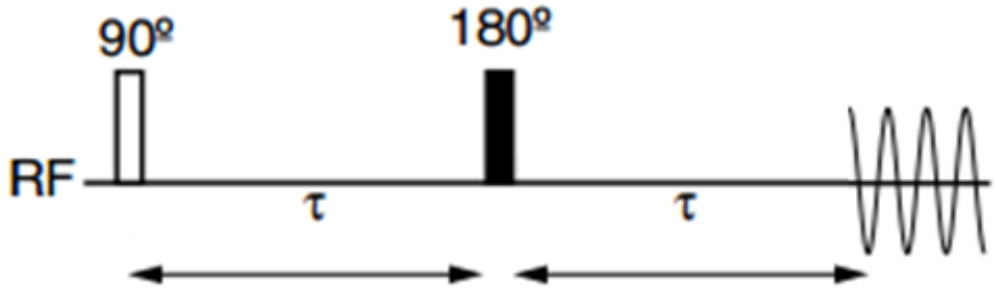

Figure 11. The pulse sequence of Spin-Echo to measure T_2 relaxation.

In theory, the spin-lattice relaxation can be treated by considering the rates of transitions of the spins between energy levels. For example, the rate constants for transition between the energy levels in the case of isotropic rotation can be expressed as:

$$W_0 = \frac{\omega_D^2}{4} J\left(\omega_I - \omega_S\right) = \frac{\omega_D^2}{10}\left\{\frac{\tau_c}{1+\left(\omega_I - \omega_S\right)^2 \tau_c^2}\right\},$$

$$W_I = \frac{3\omega_D^2}{8} J\left(\omega_I\right) = \frac{3\omega_D^2}{20}\left\{\frac{\tau_c}{1+\omega_I^2 \tau_c^2}\right\},$$

$$W_S = \frac{3\omega_D^2}{8} J\left(\omega_S\right) = \frac{3\omega_D^2}{20}\left\{\frac{\tau_c}{1+\omega_S^2 \tau_c^2}\right\},$$

$$W_2 = \frac{3\omega_D^2}{2} J\left(\omega_I + \omega_S\right) = \frac{3\omega_D^2}{5}\left\{\frac{\tau_c}{1+\left(\omega_I + \omega_S\right)^2 \tau_c^2}\right\}.$$

where, W_0 is the zero quantum ("flip-flop") transition rate in which both spins are flipped in opposite senses; W_I and W_S are the single quantum transition rates where an I spin and an S spin flip respectively; W_2 is the double quantum transition rate, in which both spins are flipped in the same sense ("flip-flip"). These transition rates can be introduced into the Solomon equations:

$$\frac{d\Delta I_z(t)}{dt} = -\left(W_0 + 2W_I + W_2\right)\Delta I_z(t) - \left(W_2 - W_0\right)\Delta S_z(t)\ ,$$
$$\frac{d\Delta S_z(t)}{dt} = -\left(W_0 + 2W_S + W_2\right)\Delta S_z(t) - \left(W_2 - W_0\right)\Delta I_z(t)$$

which implies that for a pair of interacting spins, the longitudinal relaxation of any one spin is not only dependent on the departure of its magnetization from equilibrium (auto-relaxation), but also on the departure of the magnetization from equilibrium of the other spin (cross-relaxation).[70] Spatial information obtained from a pair of coupled protons can be usually determined from the cross-relaxation and the Solomon equations are extremely useful for explication of this cross-relaxation phenomenon in structural determination process.

Though there is a complete discussion of solid-state NMR in the literature, the theory and concepts presented in this chapter were used for the experiments and will serve as a quick reference. The solid-state NMR experiments described in this project measure the temperature-dependent interactions of ice and the CH host-guest model. They can also potentially expand the current understanding of the structure and chemical dynamics of clathrate hydrates in the hydrogen bonded frame work.

4.2 Ice and Quasi Liquid Layer

Since all three common types of hydrate structures consist of about 85% water on a molecular basis, many of the hydrate mechanical properties resemble those of ice. Hexagonal ice (Ih) is the most common solid form of water, which is formed by tetrahedrally connecting four other water molecules through a hydrogen-bonding network. Thus, many properties of ice are similar to hydrates. The guest molecules are believed to have great impact on the dynamics of the hydrogen-bonding network. In the case of methane, it cannot dissolve in water at room temperature, but methane clathrate hydrates can be formed in very short time when methane is pressurized into the ice. This clearly shows that some interesting behaviors are associated with

conversion of hydrogen network from ice to clathrate hydrate. This dynamical information involving diffusion of guest molecules through ice and reordering of the ice framework to form hydrate structure is still unclear. Research has also indicated that formation of clathrate hydrate may be related to the premelt ice layer under the bulk melting point referred to as the quasi-liquid layer (QLL).[57] The presence of QLL in ice may play an important role in assisting the guest molecules in diffusing into ice and eventually reshaping the hydrogen-bonding network. The non-invasive and non-destructive nature of NMR is a very important advantage for providing dynamical information in these systems. With this in mind, we endeavored to investigate the melting behaviors of QLL in polycrystalline ice by solid-state magic angle spinning (MAS) NMR techniques as the control experiments for the future clathrate hydrate samples. By understanding the dynamics of QLL in ice, we were hoping to understand more about the interactions between guest molecules and QLL on clathrate hydrate formation.

4.2.1 Experimental Methods

Unlike the conventional MAS experiments where powdered sample is usually packed into rotors directly, most clathrate hydrates have to be formed under extreme conditions. Therefore, maintaining the sample in the initial solid phase in the fast spinning experiment is a technical challenge. Laboratory capillary tubes are used as a secondary container in the rotor for the ice experiments. In order to make a sample, a homemade aluminum capillary holder is submerged in liquid nitrogen to keep it at low temperature. The length of capillary under the liquid nitrogen surface has been measured to have enough sample volume (**Figure 12**). The sealing process is usually done by two people; one needs to ensure the bottom portion of the capillary with the sample is kept in liquid nitrogen, while the other needs to rapidly seal the upper portion with flame, otherwise the precooled sample on the bottom will be warmed up and the clathrate sample

will decompose. This experimental apparatus and technique have been tested repeatedly by successful sealing different ice samples, which essentially provide sufficient experience for the preparation of clathrate hydrate samples.

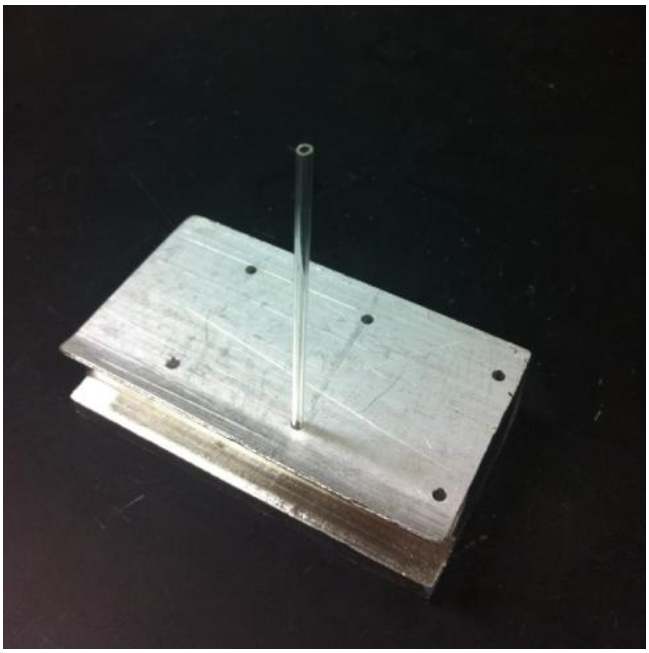

Figure 12. A picture of the aluminum capillary holder. The lower portion is trimmed down to let liquid nitrogen flow into the channel to cool down the sample .

For the NMR experiments, some hardware modifications are needed in order to meet the fast spinning and low temperature requirements for this study. In NMR, a radio frequency (RF) coil is the core part of the NMR probe. It creates the B_1 field, which rotates the net magnetization in a pulse sequence and also detects the transverse magnetization as it precesses in the X-Y plane. Because of the compact design of the NMR probe, the sample rotor needs to be inserted in the coil to receive the homogenous transmitted B_1 field. Misalignment of the RF coil may cause it to make contact with the rotor during fast spinning experiments, which causes the danger of crashing the rotor, damage and diminishing the quality of the spectra. A coil clamp was designed and installed by my co-worker Dr.Sengupta and me. This Teflon clamp is machined to be put in

a small stator with dimension of ~0.6" diameter and ~0.35" height. It takes up most of the extra space in the stator but leaves a little clearance to allow installation of the RF coil. The part is designed to reduce the space around the coil so as to reduce the misalignment of the coil when a sample is spun in the probe. **Figure 13** is the schematic of this design. Since Teflon has much lower heat capacities than air, taking up most of the empty space by Teflon also improves the efficiency of the cooling of the sample, which is essential for clathrate studies.

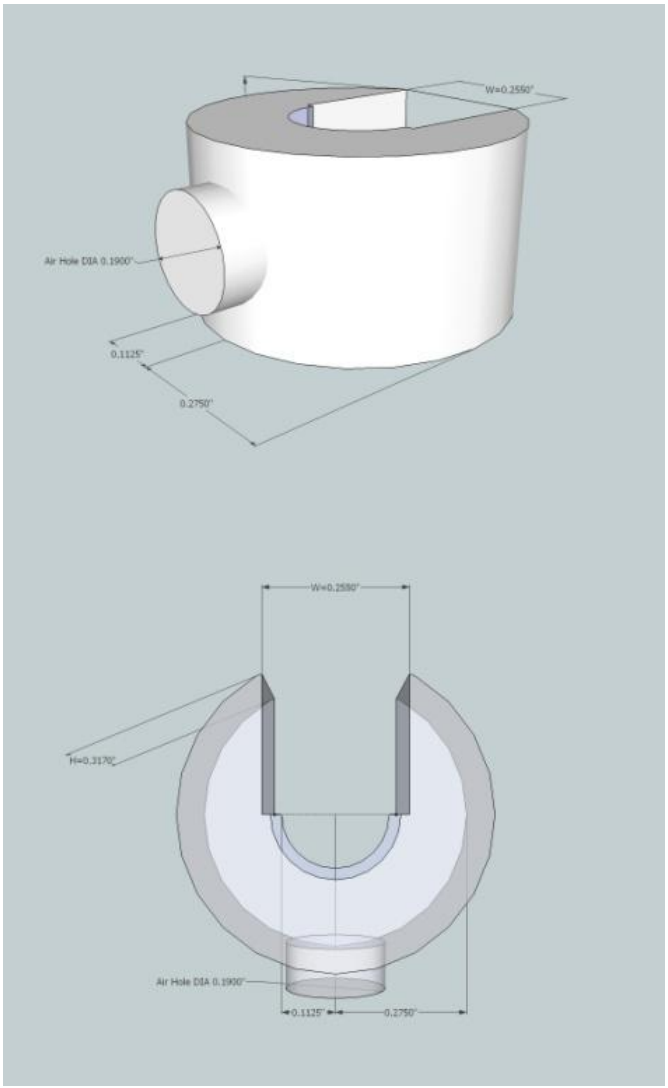

Figure 13. The top and side view of the Teflon coil clamp. The center semi-circular space provides enough room for the RF coil to be installed. The square cut-off serves as a lock-key mechanism which allows a square insert (not shown) to lock and stabilize the coil leads.

The cooling system of our MAS probe is a heat-exchange dewar.[72] It passes a stream of wall air into a spiral heat-exchange pipe in liquid nitrogen and sends the cooled air to the NMR probe via a well-insulated transfer line. This set-up can easily bring the system temperature down to -60 ℃ but did not allow us to access the desired intermediate temperature ranges with fine control. An air flow meter is installed in the air inlet which greatly increases the fine control of the temperature over the accessible range of temperature from -60 ℃ to room temperature with 2~3 ℃ increments.

4.2.2 Results and Discussion

Surprisingly there are few recent solid-state NMR studies on polycrystalline ice. Some early relevant work was conducted including measurement of proton relaxation in hexagonal ice,[73] identifying ice polymorphs by ^{1}H and ^{2}H NMR,[74] studying the mechanism of proton transportation processes,[75] and following the freezing behavior in mesoporous materials.[76]. Despite the obvious importance of the problems, research on ice is still important and needed as a control for understanding the behavior of clathrate hydrates and to investigate the differences between clathrates and ice.

We first started following the melting behavior of bulk ice by MAS NMR from -40 ℃ to 25 ℃ and we observed some questionable results. When the water is first frozen to -40 ℃, the spectrum was a broad signal because all the water molecules are trapped in the hydrogen-bonding network and randomly oriented in all possible directions. When the temperature is increased to -22 ℃, a signal at 3.5 ppm appears in the spectrum (**Figure 14**). This signal becomes more intense as temperature goes up to -7 ℃, which suggests that the signal is temperature dependent and is also associated with the melting process of the bulk ice. Another small peak starts appearing at -7 ℃ . This signal appears at 5.2 ppm, which is the chemical shift

value as bulk liquid water just above the melting point. However, the peak at 5.2 ppm is only a tenth of the room temperature signal intensity of liquid water. A possible chemical exchange phenomenon is further observed at -4 ℃ where another signal shows up at 4.5 ppm. By comparing the intensities of the other two signals at -7 ℃ and -4 ℃, the signal at 5.2 ppm is less intense at higher temperature while the 3.5 ppm remains about the same or increases slightly. We postulate that the 4.5 ppm signal might be due to a fast proton exchange between the interface of liquid water and the 3.5 ppm signal.

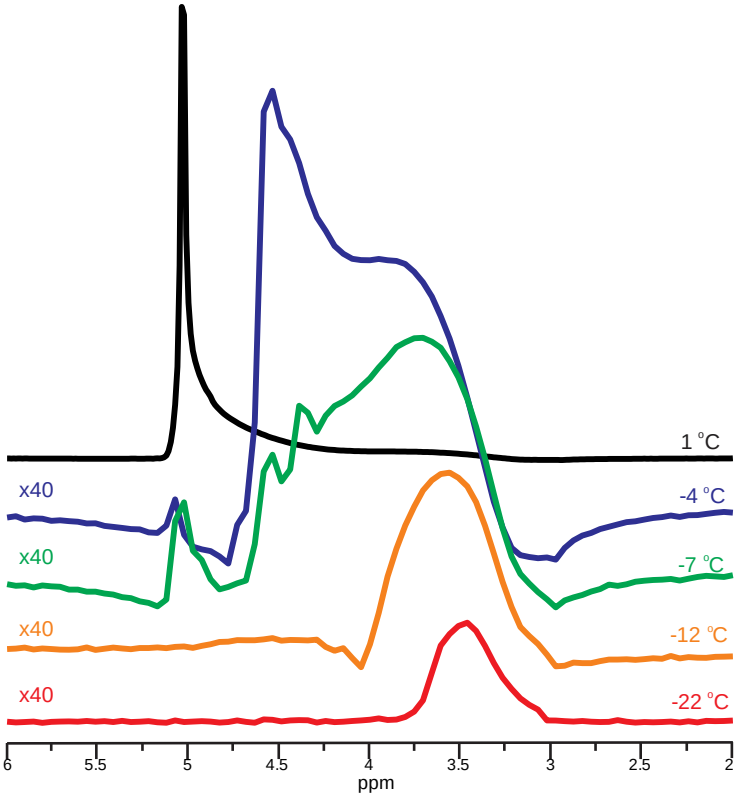

Figure 14. Melting behavior of water as a function of temperature as studied by solid-state MAS NMR.

To verify this result, we have performed some comparison experiments for validation purposes. Early static solid-state NMR measurements used diluted water with 99.5% D_2O to suppress the effect from radiation damping.[77] We have performed a series MAS experiments with varying D_2O concentration at 12.5%,70% (**Figure 15**), and 99.5%. The lineshape of the

spectrum is improved in a way with the decreased H_2O percentage due to lesser radiation damping effects, but more importantly all the signals discovered from the pure water sample are reproducible in 12.5% and 70% D_2O samples (99.5% D_2O signals does not show the 3.5 ppm and 4.5 ppm signals due to the low concentration of H_2O). We have also tested a rotor with blank capillary and a rotor containing only water (no capillary) with MAS NMR. The blank experiment shows that the background signal is extremely small and can be neglected. The results from water-only experiments are consistent with the original water and capillary sample that 3.5 ppm and 4.5 ppm signals all appear at similar temperature range, which eliminate the possibility of observing interactions between water and glass.

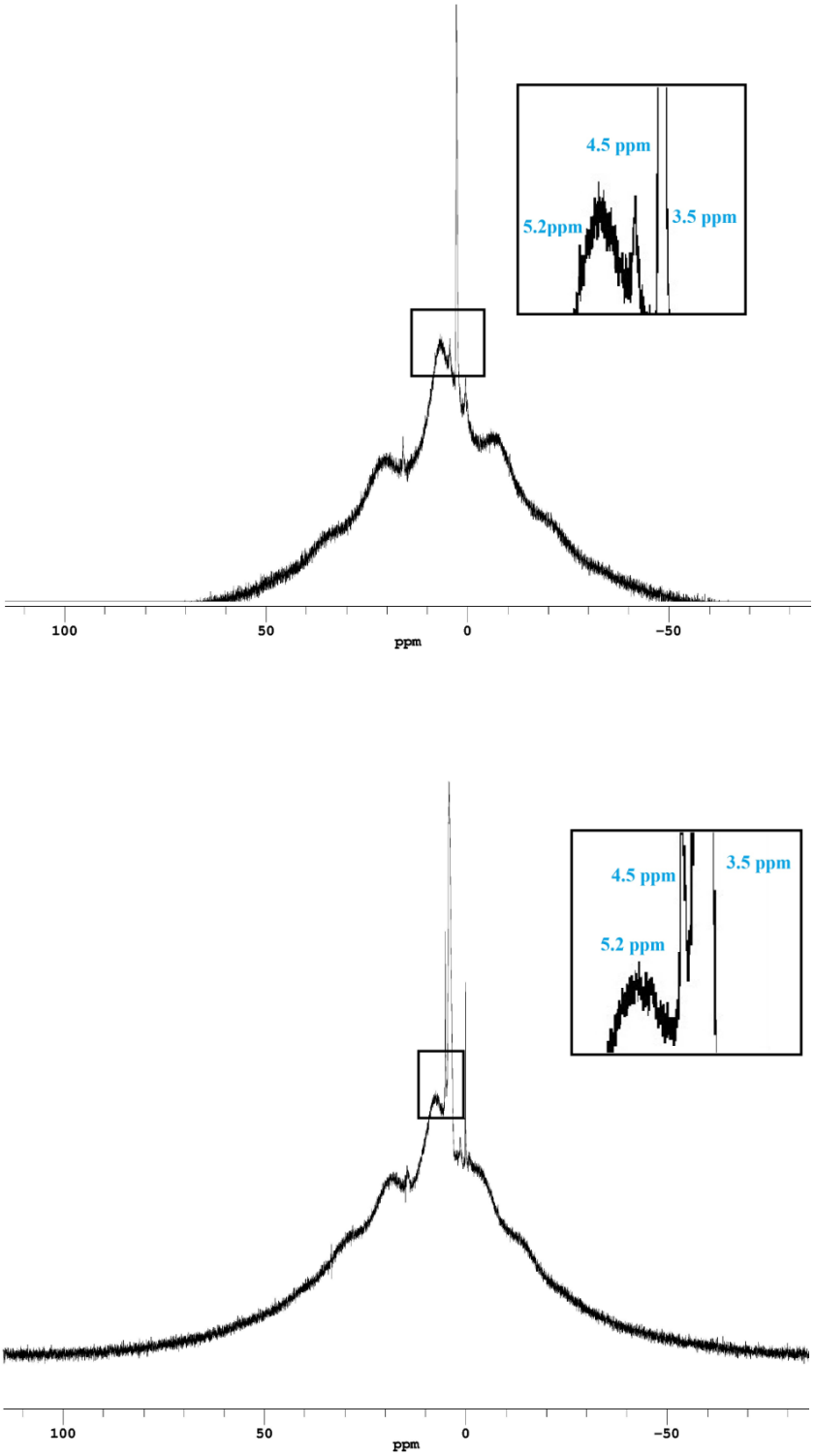

Figure 15. MAS spectra of 12.5% D_2O at -21 ℃ (top) and 70% D_2O at -4 ℃ (bottom) samples. The signals obtained here are consistent with signals observed in pure water (5.2, 4.5, & 3.5 ppm).

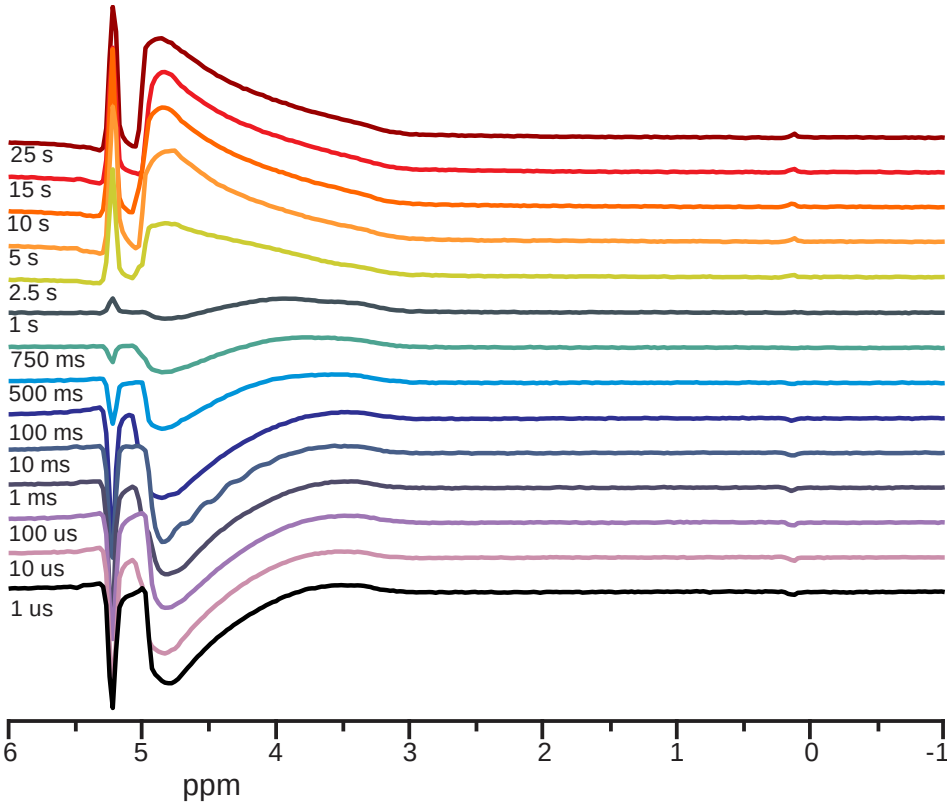

Figure 16. T_1 measurements on bulk ice at -0.5 ^{o}C.

In order to further investigate the origin of the 3.5 ppm signal in water sample, T_1 relaxation experiments have been performed by using the inversion-recovery technique at different temperatures. Below the melting point, at -0.5 ℃, the T_1 of 4.5 ppm and 5.2 ppm signals are in the order of a few seconds (**Figure 16**). However, the signal at 3.5 ppm is never inverted from the T_1 spectra and its intensity of 3.5 ppm is growing when delay time τ increases. If this phenomenon is real, it means the T_1 relaxation time of the species at 3.5 ppm is so short that the magnetization has almost relaxed back to its equilibrium state even at the shortest delay possible in our spectrometer. This questionable result encouraged us to reexamine the experiment and as we further investigated, this "fast dynamics" is due to the unbalanced cooling on the rotor.

In **Figure 17**, the sample is cooled by introducing cold air from the top of the stator. When the experiment starts, the drive air from bottom of the stator provides a levitating force to initiate the

spinning. Through the whole experiment, the drive air is at room temperature which means a temperature gradient is created between the center and the ends of the rotor (**Figure 18**). Therefore, the bottom and the top portions of the ice sample always melt faster than the center when the sample is being warmed up. As a result, a sharp water signal starts showing up at different frequency as the portion of the melt sample is not at the center of the RF coil. In other words, we were misled by the unbalanced sample cooling to believe we were measuring a signal from the QLL in our experiments.

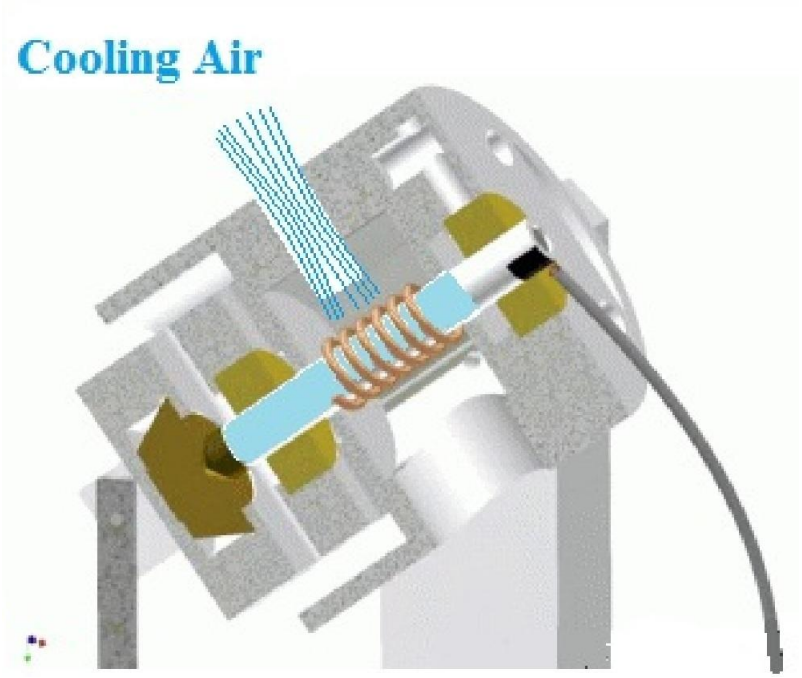

Figure 17. A schematic of cooling mechanism in the probe head.

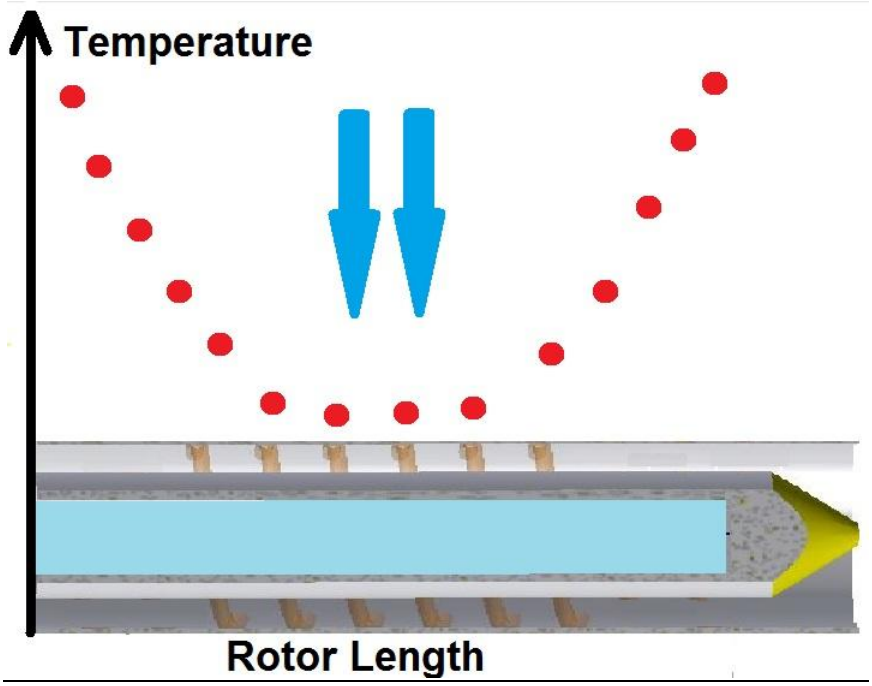

Figure 18. A temperature gradient along the rotor length from the unbalanced cooling.

4.3 Tetrahydrofuran and Cyclopentane Clathrate Hydrates

Clathrate hydrate is a unique combination of two different types of molecules: host molecules that establish the cage lattice framework and guest molecules that stabilized the lattice structure by incorporating themselves into the cages through the guest-host interactions. Typically, the guest-host interactions that stabilize the clathrate hydrate system are primary electrostatic and van de Waals forces. This is because the hydrogen bonding propensity of each water molecule in the lattice is satisfied by four neighboring water molecules. At low temperatures (below 200 K), the guest molecules are quite static and only interact weakly and nonspecifically with water molecules making up the cage. However, above 200 K, the water molecules in the lattice become more active, and hydrogen bonding between the host and guest may become more important. Nevertheless, some molecules like ethers are also capable of forming clathrate hydrates. Surprisingly, these polar guest clathrate hydrates can be formed at relatively low temperature and

at low pressure.[78–81] This is usually because of the injection of Bjerrum defects to the structure by hydrogen-bond forming guests.

In order to understand the stability and dynamics of clathrate hydrates, the guest-host interactions were both experimentally and computationally investigated. Tetrahydrofuran (THF) has been an excellent model for clathrate hydrate studies due to its ease of formation and high stability under normal atmosphere. The dynamics of THF hydrate was studied by static proton NMR and the activation energy to the motion of THF guest was extracted from spin-lattice relaxation T_1 measurements.[82] When the temperature is below 140 K, defect creation is energetically unfacorable and the activation energy is found to be 0.92 kcal/mole. As temperature increases above 200 K, the proton spin-lattice relaxation time is dominated by water reorientation motions with an activation energy of 7.2 kcal/mole. By comparing with the activation energy of ice-I_h (13.2 kcal/mole),[77] the relatively lower activation energy of water molecules in clathrate hydrate is probably due to the injections of Bjerrum defects by the guest molecules.[83] In Bjerrum defects, disorder in the water lattice is thermally induced either by having two hydrogen atoms reside between two oxygen atoms (D-defect) or no hydrogen atoms residing between two oxygen atoms (L-defect).[84] The low-temperature values for the activation energy of water and THF guest reorientation were also confirmed by deuterium and ^{17}O NMR studies at temperatures below 200 K.[85,86] The water molecule reorientation and diffusion are found to be coupled in the clathrate hydrate cage by ^2H NMR in THF·D_2O clathrate hydrate.[87] The activation energies are 12.3 kJ/mole and 24.6 kJ/mole for the two processes respectively. It is interesting to note that these values are still smaller than the activation energy of ice-I_h found by Fujara *et al.*, which are 20 kJ/mole and 50 kJ/mole respectively.[75] The observation suggests

the injections of Bjerrum L-defects on the water cages may reduce the activation energy to the water reorientation motion.

Lineshape analysis from solid echo ^{2}H experiments were also reported by Zeidler *et al.* in the same paper but the technique becomes insensitive as temperature reaches 243 K. Nevertheless, Koh and co-workers manage to identify two populations of dynamically different water molecules by using similar ^{2}H NMR techniques on THF·D_2O.[88] These two types of water molecules are related to two of the three crystallographically distinct water molecules in the CS-II structure unit cell. The values of activation energy of these two water molecules are close to each other (~ 29 kJ/mole) and they agree well with previous values reported by ^{2}H NMR.[86] Again, the lineshape analysis becomes insensitive when temperatures are much above 243 K. In addition, the dynamics of deuterated THF clathrate hydrate (TDF·H_2O) was also investigated by ^{2}H NMR.[88] From the lineshape analysis, there is a significant line width decrease of the guest near 190 K, which is the temperature at which the host water molecules enter intermediate motional regime. They also conclude that the reorientation of the guest molecule is anisotropic which may be due to deviation of the cage structure from ideal spherical geometry on the timescale of the motion of the guest.

Other clathrate hydrates were also investigated by Zeidler and co-workers including THF and CP clathrate hydrates over a temperature range from 20 K to 263 K.[89] In their report, a discrepancy in the Arrhenius behaviors of reorientation dynamics is significant at temperatures above 200 K. Therefore, the data over this temperature range is not included in the analysis. This may be attributed to the labile water molecules at higher temperatures affect the guest-host interactions. A similar ^{2}H stimulated echo experiment performed by Nelson and co-workers shows that the correlation time of cage water molecules in CP clathrate is very similar to ice-I_h

below 200 K with the same temperature dependence.[90] It indicates that the reduced lattice water reorientation barrier is more likely due to the guest-host interactions in THF and other cyclic ether clathrate hydrates.

So far, from the literature, the guest-host interactions at temperature ranges above 200 K are still not well characterized. The activation energy values for the guest orientation determined below 200 K are typically only around 1 kcal/mole, which do not appear to support hydrogen bond formation between the guest and host molecules. However, there are strong indications that polar guests are responsible for hydrogen bond formation and can also greatly change the cage water dynamics. In recent studies, hydrophilic guests play an important role in hydrogen bond formation. Buch and co-workers have shown that the clathrate can be formed at much lower temperatures and pressures by hydrogen bond forming guests.[55] Molecular dynamics simulations demonstrate that the small ether guests including THF and THP can form hydrogen bonds with cage water molecules at suitable temperatures as well.[91]

In solid state NMR, especially in Magic Angle Spinning (MAS) experiments, information regarding formation kinetics, decomposition, structural details, and inter-cage dynamics of some hydrocarbon guests can be obtained from ^{13}C solid-state NMR.[23,92–100] In this project, we demonstrate the first ^{1}H MAS NMR measurements of the correlation times and activation energies for the motion of tetrahydrofuran (C_4H_8O;THF) and cyclopentane (C_5H_{10}; CP) guests in clathrate hydrates at temperatures above 200K. Both THF and CP form CS-II clathrate structure with occupancy restricted to the large $5^{12}6^4$ cages. They are both five-membered rings of similar molecular weight, however THF has an oxygen atom with the capability of hydrogen bond formation. Therefore, the direct comparison between THF and CP clathrate hydrates will be interesting to demonstrate the possibility of host-guest hydrogen bonding. Our results show that

strong hydrogen bonding interactions are present between THF and the cage when there is significant dynamics in the host water lattice above 200 K.

4.4 Experimental Methods

Tetrahydrofuran (THF) clathrate hydrate was made by mixing 99.8% D_2O (Cambridge Isotope Laboratory,) and THF (EMD Chemical Inc.) in a stoichiometric ratio 1:17.[101] Study has shown the presence of dissolved oxygen in THF clathrate hydrate increases the proton relaxation rates and also reduce the temperature dependence of the relaxation rates. Therefore, D_2O was degassed by passing N_2 flow for two days before mixing with THF. Then the mixture of D_2O and THF was quickly dipped into liquid nitrogen to initiate the enclathration and kept in a -40 ℃ freezer for at least 48 hours. Cyclopentane (CP) is immiscible in water. Thus, the formation method of CP clathrate hydrate is slightly different from THF hydrate. CP (analytical standard, Sigma-Aldrich) was mixed with the degassed 99.8% D_2O (Cambridge Isotope) solution in 1:17 ratio. The mixture of CP and D_2O was first emulsified by ultrasonicating with Sonic Dismembrator (Fisher Scientific Model 100) at high power[102], inside a home-built glove-bag maintained under a nitrogen atmosphere to eliminate any air during the emulsification process. Then the emulsion was frozen by liquid nitrogen to initiate the enclathration and kept at 4 ℃ for at least 48 hours. In order to verify the formation of the clathrates, both THF hydrate and CP hydrate samples melting points were checked. The melting point of THF·D_2O was found to be 8 ^oC. For comparison, the melting point of a THF·H_2O hydrate sample prepared in a similar manner using deionized water, was found to have a melting point of 4 ^oC, consistent with the reported value of 4.4 ^oC.[13] For CP·D_2O sample, it was found to have two distinct melting points at 8 ^oC and 12 ^oC. For comparison, a CP·H_2O hydrate sample, prepared as above using deionized water, had a melting point of 8 ^oC, which agrees well with the literature value of 7.7 ^oC.[101] This

indicates that the CP·D_2O sample has some CP·H_2O present as impurity. In order to prevent the samples from melting and decomposing, both clathrates were carefully ground into powder and packed into 3.2 mm zirconia rotors (Revolution NMR) at -40 ℃.

NMR experiments were conducted in an 11.7 T (500 MHz proton Larmor frequency), wide-bore Oxford superconducting magnet using a Chemagnetics CMX Infinity console. For this specific sample, it was necessary to perform rapid MAS at low temperatures. Thus, a modified commercial probe from Chemagnetics was used for all experiments. The temperature was controlled using a Millrock Technologies gas chiller. The temperature was monitored using an OpSens fiber optic sensor, and the temperature was calibrated using KBr.[103] An inversion recovery sequence followed by a Hahn echo was used to measure the T_1 in the spinning samples. For the static THF·D_2O hydrate sample, the T_1 was measured using an inversion recovery sequence, followed by a solid echo.

4.5 Results and Interpretation

Due to the physical properties of clathrate hydrates as solid substances, solid-state NMR is the suitable tool for this project to make measurements of the interactions between guest and host molecules. Hopefully the results can potentially expand the current understanding of the dynamics of clathrate hydrates in the hydrogen-bonded frame work. MAS NMR has the great advantage to transform the broad signals in solid samples to high resolution liquid-like spectra. **Figure 19** is the comparison between MAS NMR and static NMR and the advantages of using MAS are clearly seen. In the spectrum, the red broad curve is a static ^1H NMR spectrum of the THF·D_2O clathrate. The blue curve is a liquid state ^1H spectrum of a 1:17 mixture THF and 99.8% D_2O at room temperature. The small peak at about 4.8 ppm is the signal from the residual water, and the peaks at 3.52 ppm and 1.78 ppm are from the THF. In this case, the two signals

from THF molecules do not appear in the static NMR measurement but are resolved by MAS with narrower line width and better signal to noise ratio in the green spectrum.

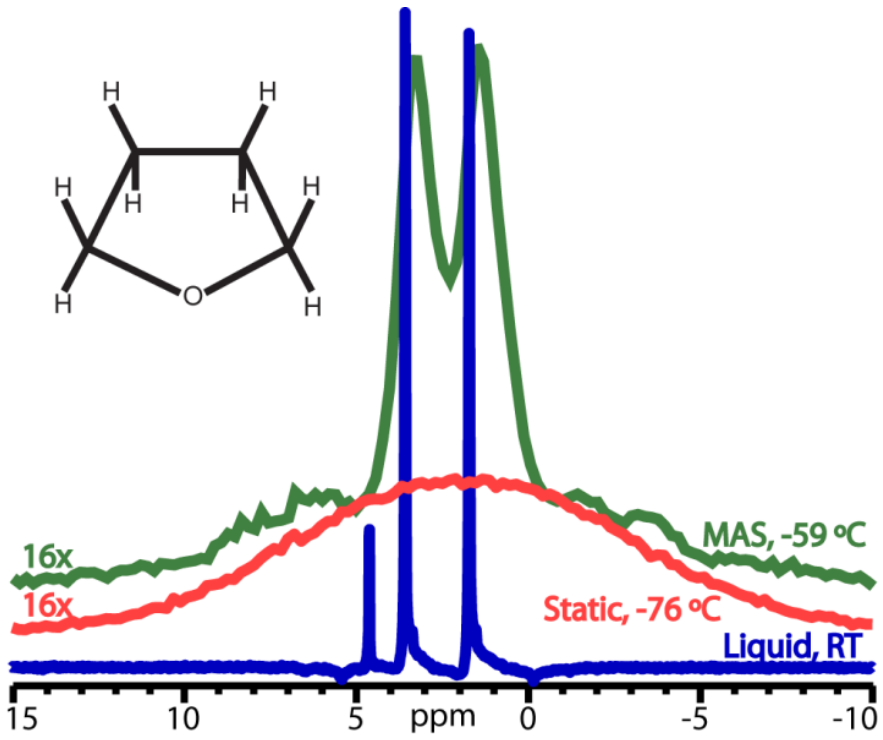

Figure 19. Comparison of liquid state 1H spectrum of 1:17 mixture of THF:99.8% D2O (blue) before hydrate formation, static NMR spectrum of THF ĐD2O hydrate (red), and MAS spectrum (green). The temperatures at which spectra were recorded are shown on the right. The hydrate spectra have been enlarged by a factor of 16 for better visualization. The small peak at 4.8 ppm in the liquid spectrum is from residual water protons. The inset shows the THF molecule.[115] Reprinted with permission from reference 115. Copyright (2015) American Chemical Society

4.5.1 Spin-lattice Relaxation Rate

Spin-lattice relaxation time (T_1) was measured by inversion recovery experiments at various temperatures. **Figure 20** shows the inversion recovery spectra obtained at 228K. The details of the pulse sequence has been discussed in previous section.

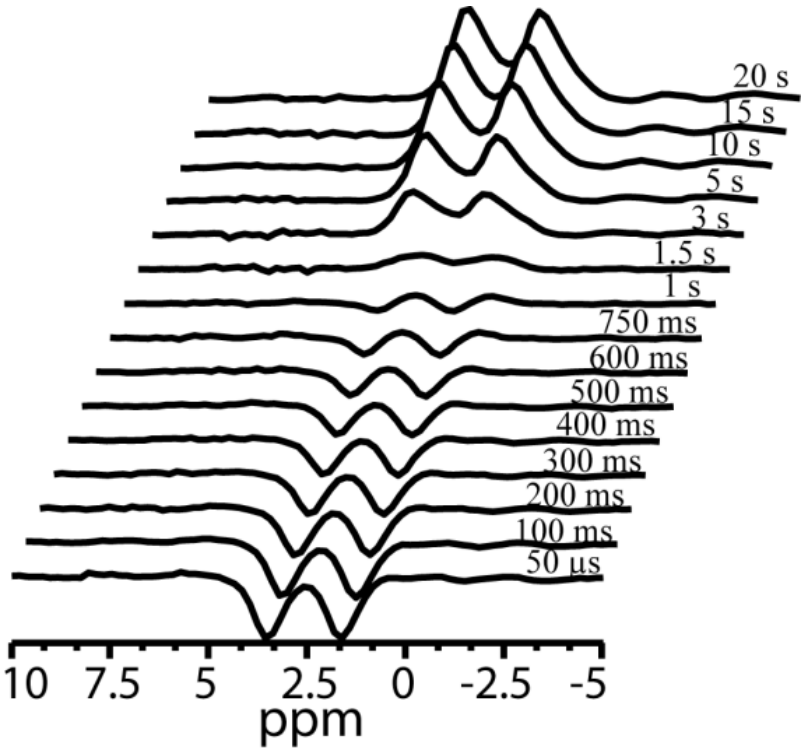

Figure 20. Inversion recovery spectra for THF:99.8% D_2O hydrate obtained at 228 K. The mixing times are indicated on the right of the spectra. As can be seen from the spectra, the two peaks have similar T_1 relaxation times.[115] Reprinted with permission from reference 115. Copyright (2015) American Chemical Society

The two distinct peaks in the THF clathrate resolved by MAS were deconvoluted and fitted individually to the equation:

$$I(t) = A\left[1 - \left\{1 - eff * \left(1 - \exp\left(-CT/T_1\right)\right)\right\}\exp\left(-t/T_1\right)\right] \qquad (1)$$

where, $I(t)$ is the intensity of the peak at a mixing time of t, eff is the efficiency of inversion, and CT is the cycle time.[104,105]

Assuming isotropic rotational motion, the spin-lattice relaxation rate, R_1 (=$1/T_1$), can be expressed in terms of spectral density functions J(ω) as:

$$R_1 = s^2 K_{IS}\left[J(\omega_0) + 4J(2\omega_0)\right] \qquad (2)$$

where ω_0 is the Larmor frequency, s^2 is the generalized order parameter, and $J(\omega) = 2\tau_c / \{5(1+\omega^2\tau_c^2)\}$, where τ_c is the correlation time for the motion. The generalized order parameter (s^2) is included to account for fast internal motions which change the experimental dipolar coupling from the theoretically calculated one. The s^2 values are also influenced by the space available for the rotating molecules. Fast librational motions dominate if s values are small which indicates the restriction of the guest molecule mobility in the cage.[89]

The factor K_{IS} is given by:

$$\frac{3}{4}\hbar^2\gamma_H^4\left(\frac{\mu_0}{4\pi}\right)^2\left\langle\frac{1}{r^6}\right\rangle \qquad (3)$$

where γ_H is the gyromagnetic ratio for protons, μ_0 is the permeability of vacuum, $\hbar$ is Planck's constant divided by 2π, and $\langle 1/r^6 \rangle$ is the average of the sixth power of the pairwise internuclear distances between all the relaxing partners normalized to the total number N of relaxing nuclei:

$$\left\langle\frac{1}{r^6}\right\rangle = \frac{1}{N}\sum_i^N\sum_{j\neq i}^N\frac{1}{r_{ij}^6}. \qquad (4)$$

For THF, because the two chemically distinct sets of protons are also resolved in chemical shift in our experiments, one needs to evaluate eq. 4 only over the protons that have the same chemical shift. Thus for the peaks at 1.78 ppm and 3.52 ppm we get K_{IS} values of 2.10×10^{10} Hz^2 and 1.74×10^{10} Hz^2 respectively.

4.5.2 Correlation Time and Activation Energy

The correlation time describes how long it takes for a molecule to rotate one radian and it also has an Arrhenius temperature dependence:

$$\tau_c = \tau_0 \exp(E_A/RT) \qquad (5)$$

where τ_0 is the correlation time at infinite temperature, and E_A is the activation barrier to the motion. By combing it with equation (2), the relaxation rate R_1 can be fitted with respect to different temperatures and the activation energy E_A will be extracted accordingly. Experimental data was acquired by MAS NMR followed by an echo sequence to eliminate the residual water signal from the clathrate sample. **Figure 21** demonstrates the spin-lattice relaxation rate R_1 with fitting. The correlation time (τ_0) at infinite temperature for signal at 1.78 ppm and 3.52 ppm are found to be $8.6 \pm 0.4 \times 10^{-14}$ s and $12.0 \pm 0.7 \times 10^{-14}$ s respectively. Thus, the activation energy E_A is extracted to be 4.7 ± 0.1 kcal/mole. Moreover, the generalized order parameters (s^2) are obtained from the fitting and they are 0.05 and 0.04 for the signal at 1.78 ppm and 3.54 ppm. Compared to literature values,[89] these order parameters are significantly smaller and the guest molecules may be severely restricted in the $5^{12}6^4$ cages of the hydrate at this range of temperature. In addition, T_1 measurements of static THF·D_2O hydrate (**Figure 20**) were conducted by using inversion recovery sequence with a solid echo for better refocusing. As expected, two THF protons signals are not resolved in the static sample in the T_1 measurements and the temperature dependence of spin-lattice relaxation is much less profound in the range that we are interested.

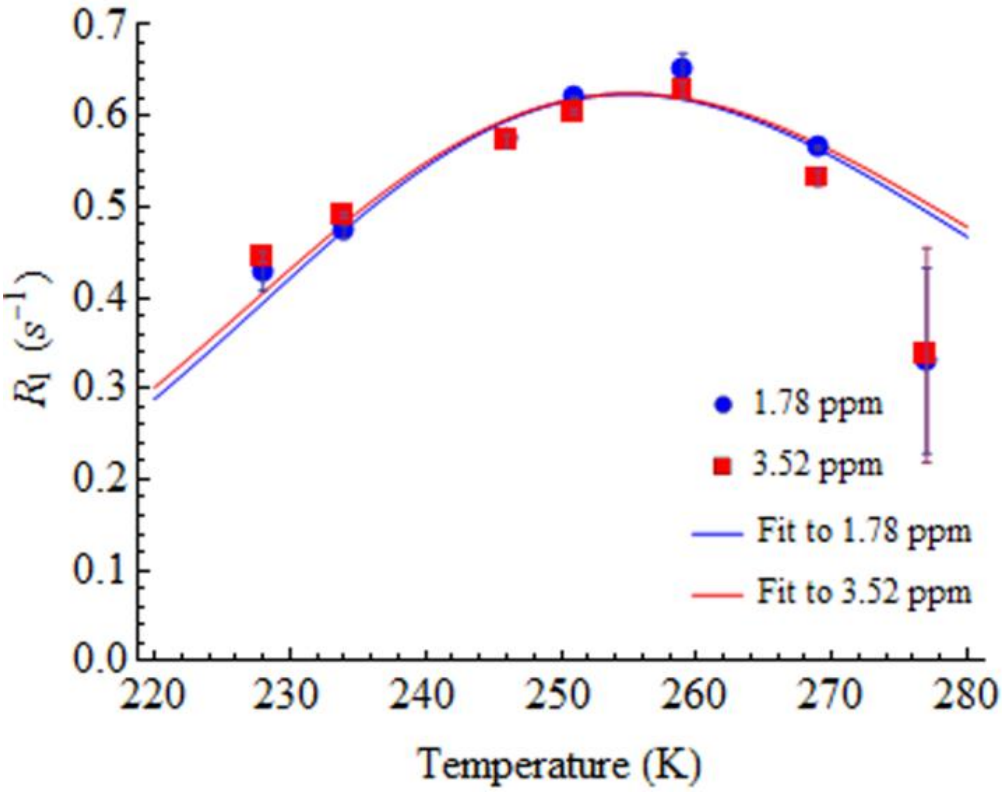

Figure 21. Relaxation rate as a function of temperature for the two peaks in the spectrum of THF clathrate. The experimental data is shown with dots, and the fit to the equations are shown with lines. The data point at 277 K has a larger error bar because it is very close to the melting point of THF hydrate and the sample was partially melted. The fits give a value of 4.7 ± 0.1 kcal/mole (19.7 ± 0.4 kJ/mole) for the activation energy, and correlation times (τ_0) of $8.6 \pm 0.4 \times 10^{-14}$ s and $12.0 \pm 0.7 \times 10^{-14}$ s for the peaks at 1.78 ppm and 3.52 ppm respectively.[115] Reprinted with permission from reference 115. Copyright (2015) American Chemical Society

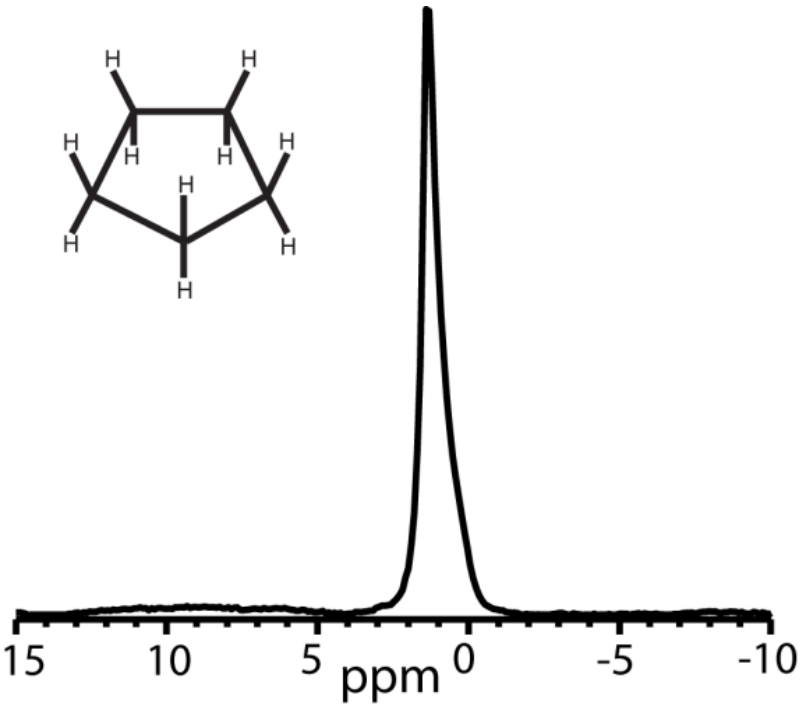

Figure 22. Cyclopentane (CP):99.8% D_2O hydrate MAS ^1H spectrum recorded at 202 K. The CP protons are not resolved in chemical shift and appear at about 1.4 ppm. Thus each proton in CP is relaxed by nine other protons, compared to THF, where each proton is relaxed by only 3 other protons.[115] The inset shows the cyclopentane molecule. Reprinted with permission from reference 115. Copyright (2015) American Chemical Society

For the other hydrate sample cyclopentane (CP), T_1 values were measured on the order of milliseconds. Compare to THF hydrate, where the T_1 is on the order of seconds, the T_1 of CP is much shorter. This is due to the different molecular structure of CP, where each proton on the ring is relaxed by nine other identical protons rather than by three distinct protons in THF (**Figure 22**). Thus, the chemical shifts of all guest protons are the same. K_{IS} is calculated to be 2.76×10^{10} Hz^2 from equation (3).

In **Figure 23**, the spin-lattice relaxation rate of CP hydrate is shown with a fitted line. The activation energy is extracted from the fitted line to be 0.67 ± 0.14 kcal/mole (2.80 ± 0.59 kJ/mole). In previous static NMR studies, Jacob *et al.* and Nelson *et al.* reported the activation energy of CP guest molecules in the large cage are ~2.6 kJ/mole and 2.4±0.3 kJ/mole respectively.[89,90] The values are close enough to what we report here. However, the trapped oxygen molecules in clathrate hydrate samples were reported to have great impacts on shortening

the spin-lattice relaxation and reducing the temperature dependence.[106] Therefore, extra efforts were taken to remove oxygen by using a homebuilt glove bag with continuous nitrogen flow while making D_2O and CP emulsion. By doing this, the effect from oxygen is believed to be diminished. Since the relaxation rate of CP hydrate does not go through an inversion, correlation times and order parameters are unable to be estimated at this temperature range.

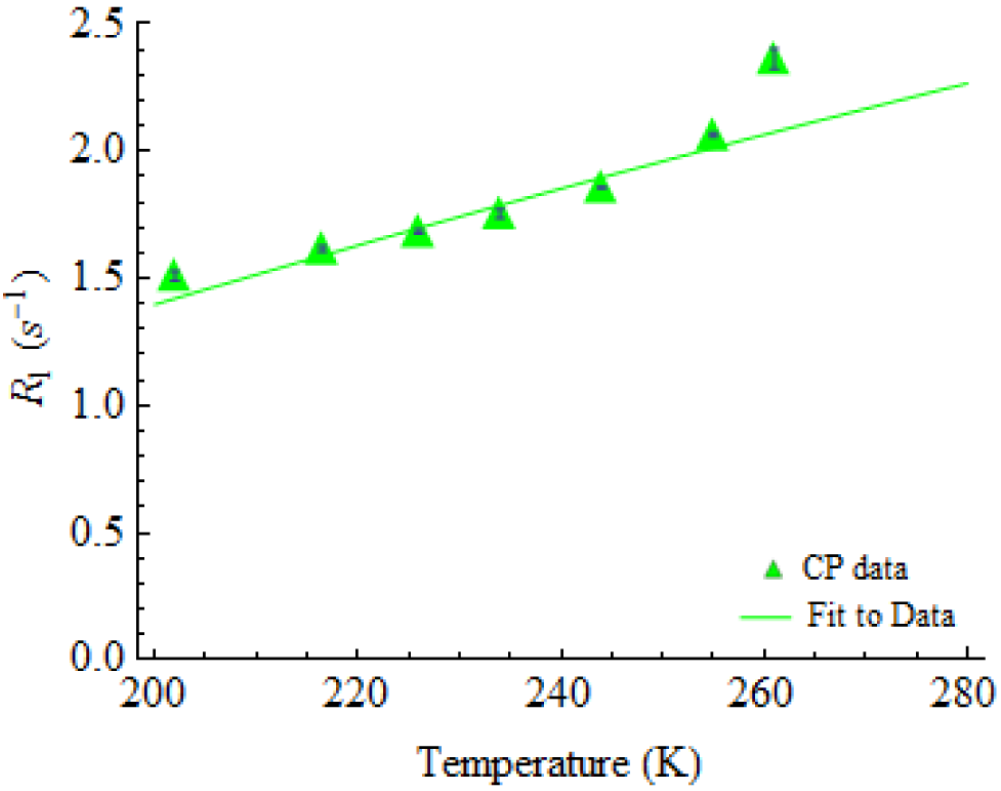

Figure 23. Spin-lattice relaxation rate for cyclopentane hydrate as a function of temperature. The fit to the data gives an activation barrier of 0.67 ± 0.14 kcal/mole (2.8 ± 0.59 kJ/mole).[115] Reprinted with permission from reference 115. Copyright (2015) American Chemical Society

Table 3 shows literature results of the activation energy to guest motion in THF and CP. For CP hydrate, the activation energy obtained above 200K (this work) shows no significant difference from the data determined at low temperature ranges.[90] However, the activation energy to the motion of the polar THF guest molecule, in the temperature we studied (above 200K), it appears to be almost five times greater than other obtained at low temperature ranges.[82,86] The

difference in activation energy between non-polar and polar guest motion clearly shows some underlying insights of hydrate dynamics and guest-host interactions which will be addressed in greater details in the next section.

Table 3. Activation Barriers to Guest Motion in THF and CP Hydrates

Sample	E_A (kJ/mole)	Temperature[a] (K)	Ref.
$THF \cdot 17H_2O$	3.85	25 – 200	82
$THF\text{-}d_8 \cdot 17H_2O$	3.85	15 – 200	86
$THF \cdot 17D_2O$	4.14[b]	14 – 135	107
$THF\text{-}d_8 \cdot 17H_2O$	2.2	143 – 213	88
$THF\text{-}d_8 \cdot 17H_2O$	4.12	50 – 100	108
$THF \cdot 17D_2O$	19.7	228 – 277	This work
$CP \cdot 17H_2O$	2.7	n. a.	109
$CP \cdot 17H_2O$	2.6	20 – 200	89
$CP\text{-}d_6 \cdot 17H_2O$	2.9	25 – 125	90
$CP \cdot 17D_2O$	2.4	20 – 200	90
$CP \cdot 17D_2O$	2.8	202 – 261	This work

[a] Temperature range over which guest motion was analyzed.

[b] From 4 – 15 K, THF molecules behave as coupled ensemble of quantum mechanical hindered oscillators with the coupling energy between two molecules being ~ 0.39 kJ/mole.[115] Reprinted with permission from reference 115. Copyright (2015) American Chemical Society

4.5.3 Discussion

The experimental data for the spin-lattice relaxation rate has shown that the guest reorientational correlation times have a stronger temperature dependence for THF hydrate than CP hydrate in the temperature range we studied. Also, the activation energy to guest motion in THF hydrate is almost five times greater than those determined in low temperature ranges but it agrees well with low temperatures experiments in CP hydrate. The most obvious distinction between these two samples is the molecular structure: THF has a strong dipole moment but CP has none. Therefore, the ability to form hydrogen bonds with the water cage network may play an important role for these interesting phenomena above 200 K.

This experiment is also believed to be the first time to apply ^{1}H MAS NMR on clathrate hydrate system. Therefore, the nature of interactions that dominates the relaxation process is quite different from the previous static NMR studies. For example, the Hamiltonians of dipolar couplings and chemical shift anisotropy are truncated under the MAS conditions. They usually do not directly affect high-field MAS NMR spectra but have contributions to the spin relaxation process. In the case of static NMR, the spectral overlap among the guest protons and between host and guest protons substantially contribute to the relaxation rate as well. The MAS spinning speed dependence of spin-lattice relaxation rates has also been investigated before for ^{13}C and ^{15}N nuclei.[110] One of the key issues is to avoid the spectral overlap with spinning side bands from other spins. For proton NMR, especially for this study on THF and CP hydrates, this requirement is met at modest spinning speeds. At 500 MHz the T_1 for the cage water molecule are very long and the reorientation of the water molecules at this temperature are in the slow motion regime. More importantly, the residual water signal from cage was removed by T_2 filter before the acquisition since this study emphasizes on the motion of the guest molecules above 200 K only.

From Arrhenius relationship, the correlation time τ of the guest motion in THF clathrate at 240 K is calculated to be ~2.2 nanoseconds. The generalized order parameter (s^2) is only about 0.04 which strongly suggests the reorientation of the guest molecule is strictly limited by the $5^{12}6^4$ cage. This may be due to the hydrogen bonds between the polar THF guest molecule and D_2O cage only allows the guest molecule to rotate about the hydrogen bond axis.

In the clathrate hydrate cage network, the hydrogen bonding requirements of the cage water molecules are completely fulfilled, so the cage structures can remain stable above the melting point of the ice structure. The density function calculation also demonstrates that the inside of the clathrates cages have a relatively uniform and low electrostatic potential.[111] This clearly indicates that the placement of polar guest molecules inside the cages may not induce any potential differences to hinder the guest motions. Therefore, the mechanisms of oxygen atom from polar molecules to from hydrogen bonds with cage protons was still an open question. However, it is important to note that water molecules in hydrate are relatively mobile in the temperature range we studied. Normally, a stable hexagonal ice (I_h) structure is constructed by having one proton between two oxygen atoms There must be some disorders in ice structure that disrupt the hydrogen bond requirements. We proposed that the Bjerrum L-defects created by the reorientations of water molecules in the cage help THF participate in hydrogen bond formation.[55]

From molecular dynamic simulations, Alavi *et al.* also show that the small ether guest molecules like THF and tetrahydropyran (THP) can form guest-host hydrogen bonds with the water hydrogen atoms in the cage due to the formation of Bjerrum L-defects.[91] The probability of forming hydrogen bonds between the guest oxygen and host hydrogen atoms is relatively small in THF clathrate and it is directly proportional to the temperature. Thus, it indicates the formation process of guest-host hydrogen bond is thermally activated. The formation enthalpy is

calculated to be around 8.3 kJ/mole. They also concluded the guest molecules must meet three requirements to form guest-host hydrogen bonds. The guest must have an electronegative atom, have a large enough molecular volume to be close to the cage water molecule, and the large dipole moment oriented towards the electronegative atom. Another computational work from Buch *et al.*, shows two defects, namely vacancy effects and interstitial defects, play major roles in hydrogen bond formation.[55] In a vacancy defect, a water molecule is removed from the host lattice which eliminates four hydrogen bonds between water molecules. Then, the dangling-H and dangling-O atoms may strongly interact with guests to be stabilized. In interstitial defects, an additional water molecule is inserted in the host lattice to create two or three more H-bond accepter sites which may be further stabilized by hydrogen-bond forming guests. All these defect stabilization may be the underlying reason why enclathration occurs at lower temperatures and pressures for hydrogen bonding guests like small ethers and H_2S compared to non-hydrogen bonding guests. Also, in the temperature range from 210-250 K, the activation energy to water diffusion is calculated to be 4.3-5.1 kcal/mol by *ab initio* molecular dynamics simulations. In the presence of hydrogen bond forming guests, the free energy barrier to defect formation was lowered by about half even though they believe their simulations are qualitative in nature.

Another DFT study was carried out by Cwiklik *et al.* to investigate guest-host hydrogen bond in ether clathrate hydrate.[112] Instead of using the $5^{12}6^4$ large cage in CS-II hydrates, an isolated $5^{12}6^2$ large cage of CS-I hydrate was chosen for their simulation. It should be also noted that they have a different observation from Alavi's work in that the water-water hydrogen bond was reformed and all initial L-defects were removed during their optimization process except for THP. They pointed out the steric factors are important as ethylene oxide has stronger guest-host hydrogen bonding than dimethyl ether. They also showed, in most cases, the guest molecules can

form weak hydrogen bonds with host water molecules but water molecule still maintains a weak hydrogen bond with the neighboring water molecules. A recent study from Alavi *et al.* observed the guest-host hydrogen bonding in tert-butylamine (tBA) with helper gas H_2S and Xe in CS-II hydrates and pinacolone + H_2S structure-H double-hydrate using X-ray diffraction.[113] An X-ray Raman scattering (XRS) study on the formation of THF hydrate was conducted by Conrad *et al.*[114] The observation on the spectra changes in different temperatures indicating the formation of guest-host hydrogen bonding.

In this work, the temperature range is limited to above 200 K, so the exact nature of guest-host interactions at low temperatures can only be speculated upon. Compared to interpretations in the literature, our view is quite similar to Cwiklik's that the presence of hydrogen-bonding guests alone is not sufficient enough to generate Bjerrum L-defects and the dynamics of host lattice also plays an important role for strong hydrogen bond formation.[112] It is important to note that the activation energy for hydrogen-bonding guest reorientation is only marginally higher than non-polar guests; this probably indicates only weak hydrogen bonding interactions occur at temperatures below 200 K. This then opens up the question as to why the host reorientation barriers in clathrate hydrates of H-bonding guests is substantially lower than that of ice-I_h while the barriers for non-polar guests (such as CP) are comparable to ice. In our opinion, the lower reorientation barrier of ether guest molecules at low temperatures in not due to the formation of Bjerrum defects by the guest, but rather due to the stabilization of vacancy defects, and interstitial defects, as described by Buch *et al.*,[55] through weak H-bonding interactions as seen by Cwiklick *et al.*.[112]

4.6 Conclusion

The guest dynamics of THF and CP clathrate hydrates have been studied by solid-state MAS NMR in the temperature range of 200 - 275 K. In the large $5^{12}6^4$ cages of the CS-II structure, the reorientation barrier for THF clathrate hydrate is about 4.7 kcal/mole (19.7 kJ/mole), which is much higher than that for CP or previous literature values of THF at lower temperatures. This is because the lattice water is labile above 200 K and are thus available to form strong hydrogen bonds with THF. The generalized order parameter s^2 of the THF clathrate hydrate is about 0.04, which strongly indicates the guest motion is strictly limited by the cage. The results are consistent with the work reported by Devlin *et al.* that the hydrogen bonds formed by ethers or methanol plays an important role in guest-host dynamics at higher temperatures. In contrast, the activation energy to the reorientation of CP is independent of temperature range we studied. This agrees well with the hypothesis that the interaction between the guest and host is dominated by the van der Waal's interactions for non-polar molecules. So far, the dynamics of guest and the strength of the guest-host hydrogen bonding had not previously been quantitatively measured at these temperatures. Therefore, it is crucial to know these parameters to further understand the stability of clathrate hydrates. A thorough study of the energetics and dynamics of the guest-host interactions, especially at temperatures near their melting point, will greatly help in better characterizing these systems.

Bibliography

(1) Moss, G. P.; Smith, P. A. S.; Tavernier, D. Glossary of Class Names of Organic Compounds and Reactivity Intermediates Based on Structure (IUPAC Recommendations 1995). *Pure Appl. Chem.* **1995**, *67* (8–9), 1307–1375.

(2) Davy, H. The Bakerian Lecture: On Some of the Combinations of Oxymuriatic Gas and Oxygene, and on the Chemical Relations of These Principles, to Inflammable Bodies. *Trans. R. Soc. London* **1811**.

(3) Roozeboom, H. Sur L'hydrate de L'acide Sulfureux. *Recl. des Trav. Chim. des Pays*-**1884**.

(4) Williams, K. D.; Devlin, J. P. P. Formation and Spectra of Clathrate Hydrates of Methanol and Methanol-Ether Mixtures. *J. Mol. Struct.* **1997**, *416* (1–3), 277–286.

(5) Makiya, T.; Murakami, T.; Takeya, S.; Sum, A. Synthesis and Characterization of Clathrate Hydrates Containing Carbon Dioxide and Ethanol. *Phys. Chem.* **2010**.

(6) Ripmeester, J.; Ratcliffe, C. Xenon-129 NMR Studies of Clathrate Hydrates: New Guests for Structure II and Structure H. *J. Phys. Chem.* **1990**.

(7) Alavi, S.; Takeya, S.; Ohmura, R.; Woo, T. K.; Ripmeester, J. A. Hydrogen-Bonding Alcohol-Water Interactions in Binary Ethanol, 1-Propanol, and 2-Propanol+methane Structure II Clathrate Hydrates. *J. Chem. Phys.* **2010**, *133* (7).

(8) Sloan, E. D. Fundamental Principles and Applications of Natural Gas Hydrates. *Nature* **2003**, *426* (November), 353.

(9) Englezos, P. Clathrate Hydrates. *Ind. Eng. Chem. Res.* **1993**, *32* (7), 1251–1274.

(10) Jr, E. S.; Koh, C. *Clathrate Hydrates of Natural Gases*; 2007.

(11) Mak, T.; McMullan, R. Polyhedral Clathrate Hydrates. X. Structure of the Double Hydrate

of Tetrahydrofuran and Hydrogen Sulfide. *J. Chem. Phys.* **1965**.

(12) Kirchner, M.; Boese, R.; Billups, W. Gas Hydrate Single-Crystal Structure Analyses. *J. Am.* **2004**.

(13) Gough, S. R. S.; Davidson, D. W. Composition of Tetrahydrofuran Hydrate and the Effect of Pressure on the Decomposition. *Can. J. Chem.* **1971**, *49* (16), 2691–2699.

(14) Davidson, D.W., Handa, Y.P. Crystallographic Studies of Clathrate Hydrates. Part I. *Cryst. Liq. …* **1986**.

(15) Davidson, D.; Handa, Y.; Ratcliffe, C.; Tse, J. The Ability of Small Molecules to Form Clathrate Hydrates of Structure II. **1984**.

(16) Ripmeester, J.; John, S.; Ratcliffe, C.; Powell, B. A New Clathrate Hydrate Structure. *Nature* **1987**.

(17) Udachin, K.; Ratcliffe, C.; Enright, G. Structure H Hydrate: A Single Crystal Diffraction Study of 2, 2-Dimethylpentane ·5 (Xe, H2S) ·34H2O. *Supramolecular* **1997**.

(18) Rath, B. B. Methane Hydrates: An Abundance of Clean Energy? *MRS Bull.* **2008**, *33* (4), 323–325.

(19) Hammerschmidt, E. G. Formation of Gas Hydrates in Natural Gas Transmission Lines. *Ind. Eng. Chem.* **1934**, *26* (8), 851–855.

(20) Demirbas, A. Methane Hydrates as Potential Energy Resource: Part 1–Importance, Resource and Recovery Facilities. *Energy Convers. Manag.* **2010**.

(21) Kelland*, M. A. History of the Development of Low Dosage Hydrate Inhibitors. **2006**.

(22) Lee, J. D.; Englezos, P. Unusual Kinetic Inhibitor Effects on Gas Hydrate Formation. *Chem. Eng. Sci.* **2006**, *61* (5), 1368–1376.

(23) Kumar, R.; Lee, J. D.; Song, M.; Englezos, P. Kinetic Inhibitor Effects on

Methane/propane Clathrate Hydrate-Crystal Growth at the Gas/water and Water/n-Heptane Interfaces. *J. Cryst. Growth* **2008**, *310* (6), 1154–1166.

(24) Sharifi, H.; Englezos, P. Accelerated Hydrate Crystal Growth in the Presence of Low Dosage Additives Known as Kinetic Hydrate Inhibitors. *J. Chem. Eng. Data* **2015**, *60* (2), 336–342.

(25) Koh, C.; Westacott, R.; Zhang, W.; Hirachand, K. Mechanisms of Gas Hydrate Formation and Inhibition. *Fluid Phase* **2002**.

(26) Koh, C. A.; Davy, H.; Faraday, M.; Udachin, K. A.; Ratcliffe, C. I.; Ripmeester, J. A.; McMullan, R. K.; Jeffrey, G. A.; Mak, K. T.; McMullan, R. K.; et al. Towards a Fundamental Understanding of Natural Gas Hydrates. *Chem. Soc. Rev.* **2002**, *31* (3), 157–167.

(27) Nakayama, H.; Hashimoto, M. Hydrates of Organic Compounds. V. The Clathrate Hydration of Alcohols. *Bull. Chem. Soc. Jpn.* **1980**, *53* (9), 2427–2433.

(28) Davidson, D. W.; Gough, S. R.; Ripmeester, J. A.; Nakayama, H. The Effect of Methanol on the Stability of Clathrate Hydrates. *Can. J. Chem.* **1981**, *59* (17), 2587–2590.

(29) Koga, K.; Tanaka, H.; Nakanishi, K. On the Stability of Clathrate Hydrates Encaging Polar Guest Molecules: Contrast in the Hydrogen Bonds of Methylamine and Methanol Hydrates. *Mol. Simul.* **1994**, *12* (3–6), 241–252.

(30) Murthy*, S. S. N. Detailed Study of Ice Clathrate Relaxation: Evidence for the Existence of Clathrate Structures in Some Water−Alcohol Mixtures. **1999**.

(31) Blake, D.; Allamandola, L.; Sandford, S.; Hudgins, D.; Freund, F. Clathrate Hydrate Formation in Amorphous Cometary Ice Analogs in Vacuo. *Science* **1991**, *254*, 548–551.

(32) Hudson, R. L.; Moore, M. H. Far-Infrared Investigations of a Methanol Clathrate Hydrate

- Implications for Astronomical Observations. *Astrophys. J.* **1993**, *404*, L29.

(33) Devlin, J. P.; Monreal, I. A. Clathrate–hydrate Ultrafast Nucleation and Crystallization from Supercooled Aqueous Nanodroplets. *Chem. Phys. Lett.* **2010**, *492* (1), 1–8.

(34) McLaurin, G.; Shin, K.; Alavi, S.; Ripmeester, J. A. Antifreezes Act as Catalysts for Methane Hydrate Formation from Ice. *Angew. Chemie - Int. Ed.* **2014**, *53* (39), 10429–10433.

(35) Devlin, J. P. Catalytic Activity of Methanol in All-Vapor Subsecond Clathrate-Hydrate Formation. *J. Chem. Phys.* **2014**, *140* (16), 164505.

(36) Shin, K.; Udachin, K. A.; Moudrakovski, I. L.; Leek, D. M.; Alavi, S.; Ratcliffe, C. I.; Ripmeester, J. A. Methanol Incorporation in Clathrate Hydrates and the Implications for Oil and Gas Pipeline Flow Assurance and Icy Planetary Bodies. *Proc. Natl. Acad. Sci. U. S. A.* **2013**, *110* (21), 8437–8442.

(37) Wallqvist, A. On the Stability of Type I Gas Hydrates in the Presence of Methanol. *J. Chem. Phys.* **1992**, *96* (7), 5377.

(38) Shin, K.; Moudrakovski, I. L.; Davari, M. D.; Alavi, S.; Ratcliffe, C. I.; Ripmeester, J. A.; Yasuda, K.; Udachin, K. A.; Alavi, S.; Ripmeester, J. A.; et al. Crystal Engineering the Clathrate Hydrate Lattice with NH_4F. *CrystEngComm* **2014**, *16* (31), 7209–7217.

(39) Bobev, S.; Tait, K. T. Methanol—inhibitor or Promoter of the Formation of Gas Hydrates from Deuterated Ice? *Am. Mineral.* **2004**, *89* (8–9), 1208–1214.

(40) Abbondondola, J. A.; Fleischer, E. B.; Janda, K. C. Propane Clathrate Hydrate Formation Accelerated by Xenon. *J. Phys. Chem. C* **2009**, *113* (11), 4717–4720.

(41) Rivera, J. J.; Janda, K. C. Ice Particle Size and Temperature Dependence of the Kinetics of Propane Clathrate Hydrate Formation. *J. Phys. Chem. C* **2012**, *116* (36), 19062–19072.

(42) Nguyen, M. T.; Amtawong, J.; Smoll, K.; Chanez, A.; Yamano, M.; Dinh, G.-B. H.; Sengupta, S.; Martin, R. W.; Janda, K. C. Gas Flow Rate and Temperature Dependence of the Kinetics of Difluoromethane Clathrate Hydrate Formation from CF 2 H 2 Gas and Ice Particles. *J. Phys. Chem. C* **2016**, *120* (16), 8482–8489.

(43) Ribeiro, C. P.; Lage, P. L. C. Modelling of Hydrate Formation Kinetics: State-of-the-Art and Future Directions. *Chem. Eng. Sci.* **2008**, *63* (8), 2007–2034.

(44) and, L. A. S.; Kirby†, S. H.; Durham‡, W. B. Polycrystalline Methane Hydrate: Synthesis from Superheated Ice, and Low-Temperature Mechanical Properties. **1998**.

(45) Jander, W. Reaktionen Im Festen Zustande Bei Höheren Temperaturen. Reaktionsgeschwindigkeiten Endotherm Verlaufender Umsetzungen. *Zeitschrift für Anorg. und Allg. Chemie* **1927**, *163* (1), 1–30.

(46) Staykova, D. K.; Kuhs, W. F.; Salamatin, A. N.; Hansen, T. Formation of Porous Gas Hydrates from Ice Powders: Diffraction Experiments and Multistage Model. *J. Phys. Chem. B* **2003**, *107* (37), 10299–10311.

(47) Yasuda, K.; Ohmura, R. Phase Equilibrium for Clathrate Hydrates Formed with Methane, Ethane, Propane, or Carbon Dioxide at Temperatures below the Freezing Point of Water. *J. Chem. Eng. Data* **2008**, *53* (9), 2182–2188.

(48) Amtawong, J.; Guo, J.; Hale, J. S.; Sengupta, S.; Fleischer, E. B.; Martin, R. W.; Janda, K. C. Propane Clathrate Hydrate Formation Accelerated by Methanol. *J. Phys. Chem. Lett.* **2016**, *7* (13), 2346–2349.

(49) Handa, Y. P. Calorimetric Determinations of the Compositions, Enthalpies of Dissociation, and Heat Capacities in the Range 85 to 270 K for Clathrate Hydrates of Xenon and Krypton. *J. Chem. Thermodyn.* **1986**, *18* (9), 891–902.

(50) Takeya, S.; Ripmeester, J. A. Dissociation Behavior of Clathrate Hydrates to Ice and Dependence on Guest Molecules. *Angew. Chem. Int. Ed. Engl.* **2008**, *47* (7), 1276–1279.

(51) Uchida, T.; Ohmura, R.; Hori, A. Critical Size for Guest Molecules to Occupy Dodecahedral Cage of Clathrate Hydrates. *J. Phys. Chem. C* **2008**, *112* (12), 4719–4724.

(52) Collins, M. J.; Ratcliffe, C. I.; Ripmeester, J. A. Nuclear Magnetic Resonance Studies of Guest Species in Clathrate Hydrates: Line-Shape Anisotropies, Chemical Shifts, and the Determination of Cage Occupancy Ratios and Hydration Numbers. *J. Phys. Chem.* **1990**, *94* (1), 157–162.

(53) Anderson, G. K. A Thermodynamic Study of the (Fluoromethane+water) System. *J. Chem. Thermodyn.* **2013**, *57*, 71–75.

(54) Demurov, A.; Radhakrishnan, R.; Trout, B. L. Computations of Diffusivities in Ice and CO[sub 2] Clathrate Hydrates via Molecular Dynamics and Monte Carlo Simulations. *J. Chem. Phys.* **2002**, *116* (2), 702.

(55) Buch, V.; Devlin, J. P.; Monreal, I. A.; Jagoda-Cwiklik, B.; Uras-Aytemiz, N.; Cwiklik, L. Clathrate Hydrates with Hydrogen-Bonding Guests. *Phys. Chem. Chem. Phys.* **2009**, *11* (44), 10245–10265.

(56) Salamatin, A. N.; Falenty, A.; Hansen, T. C.; Kuhs, W. F. Guest Migration Revealed in CO_2 Clathrate Hydrates. *Energy & Fuels* **2015**, *29* (9), 5681–5691.

(57) Shepherd, T. D.; Koc, M. A.; Molinero, V. The Quasi-Liquid Layer of Ice under Conditions of Methane Clathrate Formation. *J. Phys. Chem. C* **2012**, *116* (22), 12172–12180.

(58) PaymanPirzadeh; Kusalik, P. G. On the Role of Ice-Solution Interface in Heterogeneous Nucleation of Methane Clathrate Hydrates. In *Gas Injection for Disposal and Enhanced*

Recovery; John Wiley & Sons, Inc.: Hoboken, NJ, USA, 2014; pp 371–380.

(59) Gerlach, W.; Stern, O. Der Experimentelle Nachweis Der Richtungsquantelung Im Magnetfeld. *Zeitschrift f*[illegible]*r Phys.* **1922**, *9* (1), 349–352.

(60) Rabi, I. I.; Zacharias, J. R.; Millman, S.; Kusch, P. A New Method of Measuring Nuclear Magnetic Moment. *Phys. Rev.* **1938**, *53* (4), 318–318.

(61) Bloch, F.; Hansen, W. W.; Packard, M. Nuclear Induction. *Phys. Rev.* **1946**, *69* (3–4), 127–127.

(62) Purcell, E. M.; Torrey, H. C.; Pound, R. V. Resonance Absorption by Nuclear Magnetic Moments in a Solid. *Phys. Rev.* **1946**, *69* (1–2), 37–38.

(63) Ernst, R. R.; Anderson, W. A. Application of Fourier Transform Spectroscopy to Magnetic Resonance. *Rev. Sci. Instrum.* **1966**, *37* (1), 93.

(64) Becker, E. D. A BRIEF HISTORY OF NUCLEAR MAGNETIC RESONANCE. *Anal. Chem.* **1993**, *65* (6), 295A–302A.

(65) Abragam, A.; Hebel, L. C. The Principles of Nuclear Magnetism. *Am. J. Phys.* **1961**, *29* (12), 860.

(66) Duer, M. J. *Introduction to Solid-State NMR Spectroscopy*; Blackwell, 2004.

(67) Levitt, M. H. *Spin Dynamics Basics of Nuclear Magnetic Resonance.*; Wiley, 2013.

(68) ANDREW, E. R.; BRADBURY, A.; EADES, R. G. Nuclear Magnetic Resonance Spectra from a Crystal Rotated at High Speed. *Nature* **1958**, *182* (4650), 1659–1659.

(69) Lowe, I. J. Free Induction Decays of Rotating Solids. *Phys. Rev. Lett.* **1959**, *2* (7), 285–287.

(70) Cavanagh, J.; Fairbrother, W. J.; Palmer, A. G. I.; Rance, M.; Skelton, N. J. Relaxation and Dynamic Processes. *Protein NMR Spectrosc. Princ. Pract.* **2007**, 333–404.

(71) Hahn, E. L. Spin Echoes. *Phys. Rev.* **1950**, *80* (4), 580–594.

(72) Martin, R. W.; Zilm, K. W. Variable Temperature System Using Vortex Tube Cooling and Fiber Optic Temperature Measurement for Low Temperature Magic Angle Spinning NMR. *J. Magn. Reson.* **2004**, *168* (2), 202–209.

(73) Bruno, G. F.; Pintar, M. M. Relaxation of the Proton Spin Dipolar Energy in Hexagonal Ice. *J. Chem. Phys.* **1973**, *58* (12), 5344.

(74) Rabideau, S. W.; Finch, E. D.; Denison, A. B. Proton and Deuteron NMR of Ice Polymorphs. *J. Chem. Phys.* **1968**, *49* (10), 4660.

(75) Geil, B.; Kirschgen, T. M.; Fujara, F. Mechanism of Proton Transport in Hexagonal Ice. *Phys. Rev. B* **2005**, *72* (1), 14304.

(76) Liu, E.; Dore, J. C.; Webber, J. B. W.; Khushalani, D.; Jähnert, S.; Findenegg, G. H.; Hansen, T.; Anderson R, L. M. T. B. and B. R. W.; Anderson R, L. M. T. B. and B. R. W.; Baker J M, D. J. C. and B. P.; et al. Neutron Diffraction and NMR Relaxation Studies of Structural Variation and Phase Transformations for Water/ice in SBA-15 Silica: I. The over-Filled Case. *J. Phys. Condens. Matter* **2006**, *18* (44), 10009–10028.

(77) Wittebort, R. J.; Usha, M. G.; Ruben, D. J.; Wemmer, D. E.; Pines, A. Observation of Molecular Reorientation in Ice by Proton and Deuterium Magnetic Resonance. *J. Am. Chem. Soc.* **1988**, *110* (17), 5668–5671.

(78) Fleyfel, F.; Devlin, J. P. FT-IR Spectra of 90 K Films of Simple, Mixed, and Double Clathrate Hydrates of Trimethylene Oxide, Methyl Chloride, Carbon Dioxide, Tetrahydrofuran, and Ethylene Oxide Containing Decoupled Water-d2. *J. Phys. Chem.* **1988**, *92* (3), 631–635.

(79) Richardson, H. H.; Wooldridge, P. J.; Devlin, J. P. FT-IR Spectra of Vacuum Deposited

Clathrate Hydrates of Oxirane H2S, THF, and Ethane. *J. Chem. Phys.* **1985**, *83* (9), 4387.

(80) Fleyfel, F.; Devlin, J. P. Infrared Spectra of Large Clusters Containing Small Ether Molecules: Liquid, Crystalline, and Clathrate-Hydrate Cluster Spectra. *J. Chem. Phys.* **1990**, *92* (1), 36.

(81) Justin Hernandez; Nevin Uras, and; Devlin*, J. P. Coated Ice Nanocrystals from Water−Adsorbate Vapor Mixtures: Formation of Ether−CO2 Clathrate Hydrate Nanocrystals at 120 K. **1998**.

(82) Garg, S. . K.; Davidson, D. . W.; Ripmeester, J. . A. NMR Behavior of the Clathrate Hydrate of Tetrahydrofuran. I. Proton Measurements. *J. Magn. Reson.* **1974**, *15* (2), 295–309.

(83) Gough, S. R.; Whalley, E.; Davidson, D. W. Dielectric Properties of the Hydrates of Argon and Nitrogen. *Can. J. Chem.* **1968**, *46* (10), 1673–1681.

(84) Structure and Properties of Ice Author (S): Niels Bjerrum Reviewed Work (S): Source : Science , New Series , Vol . 115 , No . 2989 (Apr . 11 , 1952), Pp . 385-390 Published by : American Association for the Advancement of Science Stable URL : Http:/. **2013**, *115* (2989), 385–390.

(85) Ba, Y.; Ratcliffe, C. I.; Ripmeester, J. A. Quadrupolar Echo Double Resonance (QEDOR) and Solid Echo Double Resonance (SOLEDOR) NMR. *Chem. Phys. Lett.* **1999**, *299* (2), 201–206.

(86) Davidson, D. W.; Garg, S. K.; Ripmeester, J. A. NMR Behavior of the Clathrate Hydrate of Tetrahydrofuran. II. Deuterium Measurements. *J. Magn. Reson.* **1978**, *31* (3), 399–410.

(87) Kirschgen, T. M.; Zeidler, M. D.; Geil, B.; Fujara, F.; Mak, T. C. W.; McMullan, R. K.; McMullan, R. K.; Kvick, A.; Bernal, J. D.; Fowler, R. H.; et al. A Deuteron NMR Study

of the Tetrahydrofuran Clathrate Hydrate. *Phys. Chem. Chem. Phys.* **2003**, *5* (23), 5247.

(88) Bach-Vergés, M.; Kitchin, S. J.; Harris, K. D. M.; Zugic, M.; Koh, C. A. Dynamic Properties of the Tetrahydrofuran Clathrate Hydrate, Investigated by Solid State 2 H NMR Spectroscopy. *J. Phys. Chem. B* **2001**, *105* (14), 2699–2706.

(89) Jacobs, D. M.; Zeidler, M. D.; Kanert, O. Proton Magnetic Relaxation Studies of Various Guest Molecules in Clathrate Hydrates. *J. Phys. Chem. A* **1997**, *101* (29), 5241–5249.

(90) Nelson, H.; Ihrig, A.; Kahlau, R.; Kibies, P.; Kast, S. M.; Böhmer, R. Deuteron Magnetic Resonance and Dielectric Studies of Guest Reorientation and Water Dynamics in Six Clathrate Hydrates Containing Ring-Type Guests. *J. Non. Cryst. Solids* **2015**, *407*, 431–440.

(91) Alavi, S.; Susilo, R.; Ripmeester, J. A. Linking Microscopic Guest Properties to Macroscopic Observables in Clathrate Hydrates: Guest-Host Hydrogen Bonding. *J. Chem. Phys.* **2009**, *130* (17).

(92) Ripmeester, J. A.; Ratcliffe, C. I. Low-Temperature Cross-Polarization/magic Angle Spinning Carbon-13 NMR of Solid Methane Hydrates: Structure, Cage Occupancy, and Hydration Number. *J. Phys. Chem.* **1988**, *92* (2), 337–339.

(93) Desando, M. A.; Handa, Y. P.; Hawkins, R. E.; Ratcliffe, C. I.; Ripmeester, J. A. Dielectric and13C NMR Studies of the Carbon Monoxide Clathrate Hydrate. *J. Incl. Phenom. Mol. Recognit. Chem.* **1990**, *8* (1–2), 3–16.

(94) Rovetto, L. J.; Bowler, K. E.; Stadterman, L. L.; Dec, S. F.; Koh, C. A.; Sloan, E. D. Dissociation Studies of CH4–C2H6 and CH4–CO2 Binary Gas Hydrates. *Fluid Phase Equilib.* **2007**, *261* (1), 407–413.

(95) Steven F. Dec, *; Kristen E. Bowler; Laura L. Stadterman; Carolyn A. Koh, and; E.

Dendy Sloan, J. NMR Study of Methane + Ethane Structure I Hydrate Decomposition. **2007**.

(96) Subramanian, S.; Kini, R. A.; Dec, S. F.; Sloan, E. D. Evidence of Structure II Hydrate Formation from Methane+ethane Mixtures. *Chem. Eng. Sci.* **2000**, *55* (11), 1981–1999.

(97) Lee, J.-W.; Lu, H.; Moudrakovski, I. L.; Ratcliffe, C. I.; Ohmura, R.; Alavi, S.; Ripmeester, J. A. ^{13} C NMR Studies of Hydrocarbon Guests in Synthetic Structure H Gas Hydrates: Experiment and Computation. *J. Phys. Chem. A* **2011**, *115* (9), 1650–1657.

(98) Kida, M.; Hori, A.; Sakagami, H.; Takeya, S.; Kamata, Y.; Takahashi, N.; Ebinuma, T.; Narita, H. ^{13} C Chemical Shifts of Propane Molecules Encaged in Structure II Clathrate Hydrate. *J. Phys. Chem. A* **2011**, *115* (5), 643–647.

(99) Kida, M.; Sakagami, H.; Takahashi, N.; Nagao, J. Chemical Shift Changes and Line Narrowing in ^{13} C NMR Spectra of Hydrocarbon Clathrate Hydrates. *J. Phys. Chem. A* **2013**, *117* (20), 4108–4114.

(100) Trueba, A. T.; Kroon, M. C.; Peters, C. J.; Moudrakovski, I. L.; Ratcliffe, C. I.; Alavi, S.; Ripmeester, J. A. Inter-Cage Dynamics in Structure I, II, and H Fluoromethane Hydrates as Studied by NMR and Molecular Dynamics Simulations. *J. Chem. Phys.* **2014**, *140* (21), 214703.

(101) Davidson, D. W. Clathrate Hydrates. In *Water: A Comprehensive Treatise*; Franks, F., Ed.; Plenum Press: New York, 1973; pp 115–234.

(102) Zhang, Y.; Debenedetti, P. G.; Prud'homm, R. K.; Pethica, B. A. Differential Scanning Calorimetry Studies of Clathrate Hydrate Formation. *J. Phys. Chem. B* **2004**, *108* (43), 16717–16722.

(103) Thurber, K. R.; Tycko, R. Measurement of Sample Temperatures under Magic-Angle

Spinning from the Chemical Shift and Spin-Lattice Relaxation Rate of 79Br in KBr Powder. *J. Magn. Reson.* **2009**, *196* (1), 84–87.

(104) Canet, D.; Levy, G. C.; Peat, I. R. Time Saving in 13C Spin-Lattice Relaxation Measurements by Inversion-Recovery. *J. Magn. Reson.* **1975**, *18*, 199–204.

(105) Kowalewski, J.; Levy, G. C.; Johnson, L. F.; Palmer, L. A Three-Parameter Non-Linear Procedure for Fitting Inversion-Recovery Measurements of Spin-Lattice Relaxation Times. *J. Magn. Reson.* **1977**, *26*, 533–536.

(106) Ripmeester, J. .; Garg, S. .; Davidson, D. . NMR Behavior of the Clathrate Hydrate of Tetrahydrofuran. III. Effect of Oxygen. *J. Magn. Reson.* **1980**, *38* (3), 537–544.

(107) Albayrak, C.; Zeidler, M. D.; Küchler, R.; Kanert, O. NMR Relaxation of Tetrahydrofuran in Clathrate Hydrate. *Berichte der Bunsengesellschaft für Phys. Chemie* **1989**, *93* (10), 1119–1122.

(108) Nowaczyk, A.; Geil, B.; Schildmann, S.; Böhmer, R. Guest Motion in Tetrahydrofuran Clathrate Hydrate Studied by Deuteron Nuclear Magnetic Resonance. *Phys. Rev. B* **2009**, *80* (14), 144303.

(109) Davidson, D. W.; Ripmeester, J. A. NMR, NQR and Dielectric Properties of Clathrates. In *Inclusion Compounds*; Atwood, J. L., Davies, J. E. D., MacNicol, D. D., Eds.; Academic Press: Orlando, FL, 1984; pp 69–128.

(110) Fry, E. A.; Sengupta, S.; Phan, V. C.; Kuang, S.; Zilm, K. W. CSA-Enabled Spin Diffusion Leads to MAS Rate-Dependent T1's at High Field. *J. Am. Chem. Soc.* **2011**, *133* (5), 1156–1158.

(111) Fleischer, E. B.; Janda, K. C. Prediction of Clathrate Structure Type and Guest Position by Molecular Mechanics. *J. Phys. Chem. A* **2013**, *117* (19), 4001–4010.

(112) Kulig, W.; Kubisiak, P.; Cwiklik, L. Steric and Electronic Effects in the Host-Guest Hydrogen Bonding in Clathrate Hydrates. *J. Phys. Chem. A* **2011**, *115* (23), 6149–6154.

(113) Alavi, S.; Udachin, K.; Ripmeester, J. A. Effect of Guest-Host Hydrogen Bonding on the Structures and Properties of Clathrate Hydrates. *Chem. - A Eur. J.* **2010**, *16* (3), 1017–1025.

(114) Conrad, H.; Lehmkühler, F.; Sternemann, C.; Sakko, A.; Paschek, D.; Simonelli, L.; Huotari, S.; Feroughi, O.; Tolan, M.; Hämäläinen, K. Tetrahydrofuran Clathrate Hydrate Formation. *Phys. Rev. Lett.* **2009**, *103* (21), 218301.

(115) Sengupta, S.; Guo, J.; Janda, K. C.; Martin, R. W. Exploring Dynamics and Cage-Guest Interactions in Clathrate Hydrates Using Solid-State NMR. *J. Phys. Chem. B* **2015**, *119* (50), 15485–15492.